AALTO UNIVERSITY
SCHOOL OF SCIENCE
Engineering physics and mathematics

PHYS-E0441
Physics special assignment

Work started:	01.08.2016
Work submitted for approval:	-.-.-

Simulation of the Dispersion of Electromagnetic Waves in Plasma With a Fully Kinetic PIC Model

Miika Mäkelä
350 624

Instructor:	Markku Alho
Supervisor:	Esa Kallio

Acceptance

Date __.__.______ Grade ____

Accepted by ________________________________

AALTO UNIVERSITY
SCHOOL OF SCIENCE

ABSTRACT OF THE
SPECIAL ASSIGNMENT

Author: Miika Mäkelä

Title: Simulation of the Dispersion of Electromagnetic Waves in Plasma With a Fully Kinetic PIC Model

Date: 26.4.2017 Language: English Number of pages: 6+39

Degree programme:

Supervisor and advisor:

In this special assignment, the accuracy of a fully–kinetic particle–in–cell simulation model is studied through the dispersion of electromagnetic waves in plasma. This special assignment describes the simulation model and the physical theories behind the simulation platform. The number of possible applications for the simulation platform are noticeably increased with the addition of an absorbing boundary condition for electromagnetic waves.

The obtained dispersion relation for waves in nonmagnetized plasma agree well with the theory. Dispersion of EM waves is also studied in plasma with an external magnetic field, where the obtained dispersion relations describe the essential behaviour and closely resemble the dispersion relations predicted by theory. The macroparticle count and the addition of external magnetic field are shown to have a significant effect on the stability of the simulation.

Keywords: Dispersion, Cold plasma, Particle simulation

AALTO-YLIOPISTO PERUSTIETEIDEN KORKEAKOULU	ERIKOISTYÖN TIIVISTELMÄ

Tekijä: Miika Mäkelä

Työn nimi: Sähkömagneettisten aaltojen dispersion simuloiminen kylmässä plasmassa PIC-mallilla

Päivämäärä: 26.4.2017 Kieli: Englanti Sivumäärä: 6+39

Koulutusohjelma: Teknillinen fysiikka

Vastuuopettaja:

Työn ohjaaja: Prof Esa Kallio

Tässä erikoistyössä tarkastellaan täysin kineettisen hiukkanen–laatikossa simulaatiomallin tarkkuutta tutkimalla sähkömagneettisten (EM)-aaltojen dispersiota kylmässä plasmassa. Tämä erikoistyö kuvaa simulaatiomallin toimintaperiaatteita ja simulaatoon taustalla olevaa fysiikkaa. Simulaatiomallin mahdollisia sovelluskohteita on lisätty huomattavasti lisäämällä simulaatioon absorboivat reunaehdot EM-aalloille.

Simuloidut dispersiorelaatiot aalloille plasmassa ilman ulkoista magneettikenttää vastaavat tarkasti teorian ennustamaa dispersiota. Plasmassa ulkoisen magneettikentän kanssa, simulaatioista lasketut dispersiorelaatiot ovat saman suuntaisia, kuin teorian ennustamat, mutta eroavat teorian relaatioista jonkin verran. Solussa olevien makropartikkelien määrän ja ulkoisen magneettikentän osoitetaan vaikuttavan suuresti simulaation stabiilisuuteen.

Avainsanat: Dispersio, Kylmä plasma, Hiukkassimulaatio

Contents

Symbols and abbreviations

Symbols

Symbol	Unit	Explanation
q_s	C	Charge of a charge species s
m_s	kg	Mass of a charge species s
n_s	m^{-3}	Number density of a charge species s
$\mathbf{u}_s$	ms^{-1}	Bulk velocity of a charge species s
ω_{ps}	$rads^{-1}$	Plasma frequency of a charge species s
ω_{cs}	$rads^{-1}$	Gyro frequency of a charge species s
$\mathbf{B}$	T	Magnetic flux density
$\mathbf{E}$	Vm^{-1}	Electric field strength
$\mathbf{J}$	A	Current
ω	$rads^{-1}$	Angular frequency
$k = 2\pi/\lambda$	m^{-1}	Amplitude of a wave vector
c	ms^{-1}	Speed of light in vacuum
$n = ck/\omega$	1	Index of refraction
$\vec{K}$	-	Dielectric tensor
$\vec{\sigma}$	-	Resistivity tensor

Abbreviations

Abbreviation	Explanation
FMI	Finnish meteorological institute
PIC	Particle in cell
EM	Electromagnetic
X-mode	Extraordinary wavemode
O-mode	Ordinary wavemode
FDTD	Finite-difference time-domain
PML	Perfectly matched layer
FC	Interpolation from face values to cell values
EC	Interpolation from edge values to cell values
CN	Interpolation from cell values to node values

1 Introduction

This special assignment studies the dispersion of electromagnetic (EM) waves in cold plasma using a fully–kinetic particle–in–cell (PIC) simulation model. The simulation is built on an existing hybrid simulation code, which was originally developed to study planetary plasma environments. The addition of EM waves to the original hybrid simulation platform allows a precise simulation of the propagation of EM waves in a carefully controlled plasma environment.

In the year 2017 Finland will celebrate 100 hundred years of independence. The celebrations include launching a Finland 100 cubesat to a polar orbit above Finland. The satellite payload includes a radio transmitter and receiver, for publicity and scientific purposes. The receiver will be used to listen to radio signals and to pinpoint the origins of single radio transmissions and to show the possibilities of atmospheric research by using cubesats. For this purpose, the propagation of radio waves in the ionosphere above Finland is investigated using a house made ray tracing software. While ray tracing provides results on the propagation of rays, the comparison of he propagation of the rays with a completely kinetic plasma simulation would provide further proof for the accuracy of different methods of ray propagation.

EM waves are propagated using the finite–difference time–domain method in a Yee type grid, shown in Fig. 4, where magnetic field values are stored in cell faces and electric field values in cell edges. This is a well understood simulation method for EM waves with well known error sources. The details of the FDTD method are also presented in section 3.2. The work on the simulation platform includes moving the calculation of the electric field values from the cell nodes to the cell edges for more accurate propagation of the EM wave.

In the previous version of the simulation code, the EM waves were reflected back from the edges of the simulation box. These reflections made it impossible to study time-scales larger than those related to one or two wavelengths. This made the study of dispersion of the EM waves in plasma rather complicated. Here, absorbing boundary conditions for EM waves are added to the simulation model, which allows the study of longer time-series and accurate study of the dispersion in plasma. In this special assignment, the dispersion of EM waves in nonmagnetized plasma and magnetized plasma are studied and compared to the predictions of the cold plasma theory. The obtained dispersion relation in nonmagnetized plasma accurately matches the predictions of theory. In magnetized plasma, the main features of the dispersion of ordinary and extraordinary modes are obtained. Currently, the length-scales required for atmospheric radio wave propagation are too computationally expensive to be studied with a fully kinetic simulation model. Therefore, the possibility of replacing particles with relative permittivity is also shortly studied.

2 Background

2.1 Definition of plasma

As important and typical as plasma is in the universe, there is no single definition of a plasma. According to a generic description, plasma is a gas that has been partly ionized and exhibits collective behaviour. Here, the plasma considered is always cold plasma, where thermal effects of ions and electrons are neglected. At a macroscopic scale, an equal amount of negative and positive charges exist in plasma, which is why plasma is called quasi-neutral. Here, plasma is assumed to consist of a single ion species with elementary charge $q_i = -q_e$. The plasma thus holds equal number of electrons and positively charged ions. [1]

Due to the free charges, plasma reacts strongly to external electromagnetic fields. Plasma is often characterized with plasma frequency

$$\omega_{ps} = \sqrt{\frac{n_s q_s^2}{m_s \epsilon_0}}, \tag{1}$$

where s denotes a charge species, n is the species number density, q_s the charge of the particle, m_s the mass of the particle and ϵ_0 the permittivity of free space. Plasma frequency describes the intrinsic oscillation of the charge density in plasma. The plasma frequency for electrons is magnitudes larger than that of the ions, due to the mass difference of the particles. As lighter particles, the behaviour of electrons defines the properties of a plasma to a great extent, which is why the term plasma frequency typically refers to the electron plasma frequency. For a plasma in external magnetic field, the movement of the charged particles is more restricted. The particles are able to move along the direction of the magnetic field, but are restricted to circular trajectories perpendicular to the field. This circular motion is described by the gyrofrequency

$$\omega_{cs} = \frac{q_s B}{m_s}, \tag{2}$$

where B is the strength of the external magnetic field. Both plasma frequency and the gyro frequency are important for the dispersion of electromagnetic waves inside plasma.

2.2 Waves in plasma

For a wave with multiple frequency components, a certain frequency propagates with a phase speed defined as

$$v_p = \frac{\omega}{k}, \tag{3}$$

where ω is the angular frequency of the wave and $k = \frac{2\pi}{\lambda}$ is the magnitude of the wave vector, where λ is the wavelength. It is possible that the phase velocity exceeds the speed of light c, which is, in fact, typical for electromagnetic waves in plasma.

However, the information carried by the wave propagates with wave packets with a group speed that is always lower than the speed of light

$$v_g = \frac{\partial \omega}{\partial k}. \tag{4}$$

The frequency of the wave and the wavelength are connected through a dispersion relation. Electromagnetic waves in vacuum are described by a familiar dispersion relation, $\omega = ck$. However, in a dispersive medium, such as plasma, different frequencies may propagate with different group speeds and the frequency and the wavelength of the wave are connected through a more complicated relation. The index of refraction is defined as $n = ck/\omega$. In the following sections, dispersion relations for waves in nonmagnetized and magnetized plasmas are introduced.

The propagation of the electromagnetic waves in plasma is governed by the Maxwell's equations together with the equations of motion for the charged particles in the plasma. The plasma is assumed to remain quasi-neutral, which is guaranteed by the continuation equation for charge species s

$$\frac{\partial n_s}{\partial t} + \nabla \cdot (n_s \mathbf{u}_s) = 0, \tag{5}$$

where n_s is the number density and $\mathbf{u}_s$ the bulk velocity of charge species s. The equation of motion for the particles is effected only by the electric field and Lorentz force

$$m_s \frac{\partial \mathbf{u}_s}{\partial t} = q_s(\mathbf{E} + \mathbf{u}_s \times \mathbf{B}), \tag{6}$$

where e.g. the effects of thermal pressure and collisions have been neglected. The electric and magnetic fields are connected through the Maxwell's equations

$$\nabla \times \mathbf{E} = -\frac{\partial \mathbf{B}}{\partial t} \tag{7}$$

$$\nabla \times \mathbf{B} - \frac{1}{c^2}\frac{\partial \mathbf{E}}{\partial t} = \mu_0 \mathbf{J} \tag{8}$$

$$\nabla \cdot \mathbf{E} = \frac{1}{\epsilon_0} \sum_s q_s n_s \tag{9}$$

$$\nabla \cdot \mathbf{B} = 0, \tag{10}$$

$$\mathbf{J} = \sum_s q_s n_s \mathbf{u}_s = \frac{1}{\mu_0} \vec{\sigma} \cdot \mathbf{E} \tag{11}$$

The Eq. (7) is the Maxwell-Faraday law and the Eq. (8) is the Amperè-Maxwell's law. The current is connected to the movement of charged particles through Eq. (11), where the current is the sum of all the drift currents of all charged particle species. The second order resistivity tensor $\vec{\sigma}$, which connects the current and the electric field, is introduced later. The Eqs. (9) and (10) are the Gauss' laws for electric and magnetic fields. The divergence of a magnetic field is zero and an electric field is produced by free charges.

By assuming harmonic time dependencies $E = E_0 e^{i(\mathbf{k}\cdot\mathbf{r}-\omega t)}$, differential terms can be simplified to $\nabla\cdot = ik\cdot$, $\nabla\times = ik\times$, and $\frac{\partial}{\partial t} = -i\omega$. By linearizing Eqs. (7)-(11), the homogeneous wave equation can be solved [1][2]

$$\mathbf{n}\times(\mathbf{n}\times\mathbf{E}+\vec{K}\cdot\mathbf{E}) = 0, \tag{12}$$

where $n = ck/\omega$ is the index of refraction and $\vec{K}$ is the dielectric tensor

$$\vec{K} = \vec{1} - \frac{\vec{\sigma}}{i\omega\epsilon_0}. \tag{13}$$

The behaviour of electromagnetic fields in plasma can now be reduced to a problem of solving the dielectric tensor for the different plasma environments.

2.3 Propagation in a nonmagnetized plasma

When an electromagnetic wave enters plasma, the frequency and the wavelength are no longer connected through the simple relation $\omega = c/k$. By using the homogeneous wave equation derived in the section 2.2, it is possible to predict the propagation of an EM-wave in a cold plasma without an external magnetic field, that is, in an isotropic plasma. Equation (6) simplifies to

$$m\frac{\partial\mathbf{u}}{\partial t} = q\mathbf{E}, \tag{14}$$

which simplifies to $m(-i\omega\mathbf{u}) = q\mathbf{E}$, by assuming harmonic time dependencies. By inserting the velocity into equation (11) the current can be expressed as

$$\mathbf{J} = \sum_s \frac{iq^2 n_s}{m_s\omega}\mathbf{E} \approx \frac{ie^2 n_e}{m_e\omega}\mathbf{E}, \tag{15}$$

where the contribution of the ions is magnitudes smaller than the contribution of the electrons, due to the difference between the mass of electrons and ions. From Eq. (15) the resistivity tensor can be identified as $\vec{\sigma} = \vec{1}\frac{ie^2 n_e}{m_e\omega}$, which can then be used to write the dielectric tensor

$$\vec{K} = \vec{1} - \frac{e^2 n_e}{m_e\omega^2\epsilon_0} = 1 - \frac{\omega_p^2}{\omega^2}, \tag{16}$$

where the defition of the plasma frequency Eq. (1) is used for the electron plasma frequency. With the relation $\mathbf{n} = c\mathbf{k}/\omega$ and the dielectric tensor, the homogeneous wave equation Eq. (12) simplifies to

$$c^2\mathbf{k}\times(\mathbf{k}\times\mathbf{E}) + (\omega^2-\omega_p^2)\cdot\mathbf{E} = 0. \tag{17}$$

The result is, in fact, a matrix equation. It is now possible to decide that the investigated wave is propagating in the z-direction and the corresponding wave vector is $\mathbf{k} = k\hat{\mathbf{z}}$. The set of equations in matrix form

$$\begin{bmatrix} -c^2k^2 + \omega^2 - \omega_{pe}^2 & 0 & 0 \\ 0 & -c^2k^2 + \omega^2 - \omega_{pe}^2 & 0 \\ 0 & 0 & \omega^2 - \omega_{pe}^2 \end{bmatrix} \begin{bmatrix} E_x \\ E_y \\ E_z \end{bmatrix} = 0, \tag{18}$$

which has non-trivial solutions when the determinant of the matrix is zero. The determinant of the matrix

$$(-c^2k^2 + \omega^2 - \omega_{pe}^2)^2(\omega^2 - \omega_{pe}^2) = 0, \tag{19}$$

provides two solutions. The solution $\omega = \omega_{pe}$ is a non-propagating electrostatic mode that oscillates at the plasma frequency. The electric field of the electrostatic mode is parallel to the wave vector $\mathbf{k}$ and the wave is called longitudinal.

The other root of the determinant is a solution that describes propagating waves.

$$\omega^2 = c^2k^2 + \omega_{pe}^2. \tag{20}$$

Harmonic wave form is described by an exponential function $\mathbf{E} = \mathbf{E}\,\mathrm{e}^{i(\mathbf{k}\cdot\mathbf{x} - \omega t)}$. This wave propagates to $\hat{\mathbf{z}}$-direction and the magnetic and the electric fields are perpendicular to the direction of the propagation, similar to an electromagnetic wave in a vacuum. The Eq. (20) provides a relation between the wave vector $\mathbf{k}$ and frequency ω, it is thus called the dispersion relation of nonmagnetized plasma. A closer inspection reveals that not all frequencies are able to propagate in plasma due to wave vector $\mathbf{k}$ reaching purely imaginary values

$$k = \pm\frac{1}{c}\sqrt{\omega^2 - \omega_{pe}^2}. \tag{21}$$

When the frequency of the incident wave is smaller than the plasma frequency, k is purely imaginary and the electric field becomes an exponential function. The electric field can either grow exponentially, which is unphysical without a source inside the plasma region, or decay exponentially. When the frequency of the incoming wave approaches the plasma frequency, the value of k approaches zero and the wavelength of the wave grows to infinity. This wave is not able to propagate in plasma and is reflected. The analytical solution of the dispersion relation is shown in Fig. 1, where it is compared to the dispersion relation of an EM-wave in vacuum. In higher frequencies the EM-wave in plasma approach the behaviour of an EM-wave in a vacuum.

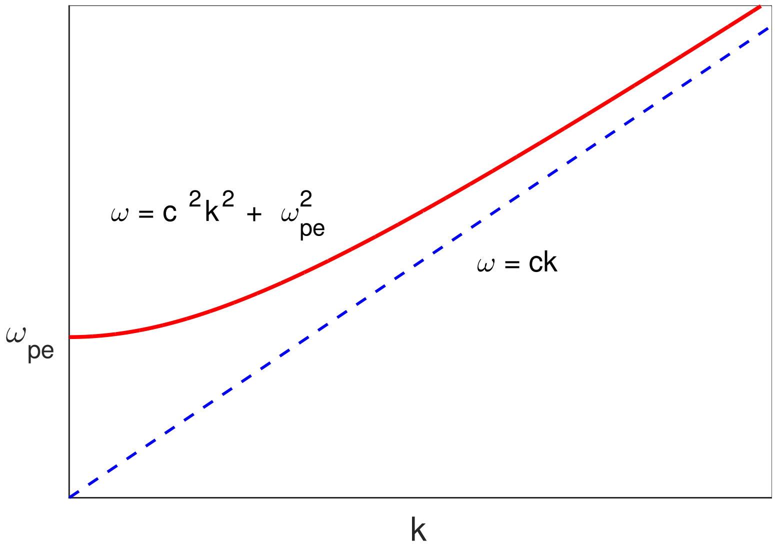

Figure 1: The possible frequencies as a function of the corresponding amplitudes of the wave vector k. The analytical solution of the dispersion relation in a nonmagnetized plasma is shown in red and the dispersion in vacuum is shown in blue.

2.4 Dispersion relation for magnetized plasma

The addition of an external magnetic field restricts the propagation of EM-waves in certain directions. The movement of the particles is not restricted parallel to the external magnetic field, but the perpendicular motion is affected by the external magnetic field. This generates new wave modes that can also have electric field components that are parallel to the direction of the propagation of the wave.

The analysis of the dispersion of the electromagnetic waves in cold plasma can be done as follows (see e.g. Cold Plasma waves [1]).The bulk flow of the charged particles follows Eq. (6) and the effects of the external magnetic field on charged particle species s are described by gyrofrequency ω_{cs}, as defined in Eq. (2). The derivation of the dielectric tensor resembles closely the derivation of the isotropic dielectric tensor. The largest difference is the second order conductivity tensor compared to the first order tensor. The derivation begins by identifying the conductivity tensor from the equations of motion (6) and once again assuming harmonic time dependencies

$$\mathbf{J} = \vec{\sigma} \cdot \mathbf{E} = \sum \frac{n_s e^2}{m_s} \begin{bmatrix} \frac{-i\omega}{\omega_{cs}^2-\omega^2} & \frac{\omega_{cs}}{\omega_{cs}^2-\omega^2} & 0 \\ -\frac{\omega_{cs}}{\omega_{cs}-\omega^2} & \frac{-i\omega}{\omega_{cs}^2-\omega^2} & 0 \\ 0 & 0 & \frac{i}{\omega} \end{bmatrix} \mathbf{E}. \tag{22}$$

The dielectric tensor is obtained from the resistivity tensor through relation in Eq. (13)

$$\vec{K} = \begin{bmatrix} S & -iD & 0 \\ iD & S & 0 \\ 0 & 0 & P \end{bmatrix}, \tag{23}$$

where the coefficients are

$$S = 1 - \sum_s \frac{\omega_{ps}^2}{\omega^2 - \omega_{cs}^2}, \quad D = \sum_s \frac{\omega_{cs}\omega_{ps}^2}{\omega(\omega^2 - \omega_{cs}^2)}, \quad P = 1 - \sum_s \frac{\omega_{ps}^2}{\omega^2}, \tag{24}$$

where the index s denotes all charged particle species. The dielectric tensor can be understood as a tensor for the relative permittivity of the plasma. The term P describes the conductivity along the external magnetic field. The term S describes the conductivity transverse to the external magnetic field and along the electric field. The term D describes the conductivity to the direction of $\mathbf{E} \times \mathbf{B}_0$. The modes can be further divided into a left-handed mode and a right-handed mode, $S = (R + L)/2$ and $D = (R - L)/2$, respectively,

$$R = 1 - \sum_s \frac{\omega_{ps}^2}{\omega^2}\left(\frac{\omega}{\omega + \omega_{cs}}\right), \quad L = 1 - \sum_s \frac{\omega_{ps}^2}{\omega^2}\left(\frac{\omega}{\omega - \omega_{cs}}\right). \tag{25}$$

The homogeneous wave Eq. (12) together with the dielectric tensor (23) give the wave equation in matrix form

$$\begin{bmatrix} S - n^2 cos^2\theta & -iD & n^2 cos\theta \sin\theta \\ iD & S - n^2 & 0 \\ n^2\cos\theta\sin\theta & 0 & P - n^2\sin^2\theta \end{bmatrix} \begin{bmatrix} Ex \\ Ey \\ Ez \end{bmatrix} = 0, \tag{26}$$

where θ is the angle between the external magnetic field and the direction of the propagation of the wave. Non-trivial solutions can be found when the determinant of the matrix is zero, which leads to dispersion equation

$$An^4 - Bn^2 + RLP = 0, \tag{27}$$

where

$$A = S\sin^2\theta + P\cos^2\theta, \quad B = RL\sin^2\theta + PS(1 + \cos^2\theta). \tag{28}$$

Solving for the angle θ from Eq. (27) reveals a different form of the dispersion relation

$$\tan^2\theta = \frac{-P(n^2 - R)(n^2 - L)}{(Sn^2 - RL)(n^2 - P)}. \tag{29}$$

For an EM-wave propagating in isotropic plasma, the dispersion relation did not depend on the direction of the propagation. In magnetized plasma differently polarized waves may only travel in certain directions. For a nonmagnetized plasma, cut-off occurs when the refractive index $n = 0$. In addition to multiple cut-off frequencies in a magnetized plasma, resonances occur when $n \to \infty$. At resonance frequency the incident wave is damped and plasma receives the energy of the wave.

2.5 Propagation of extraordinary and ordinary modes

For waves that travel perpendicular to the external magnetic field at an angle $\theta = \pi/2$, the dispersion relation Eq. (29) approaches infinity as the angle $\theta \to \pi/2$ due to the tangent function

$$\tan^2\theta = \frac{-P(n^2 - R)(n^2 - L)}{(Sn^2 - RL)(n^2 - P)} \to \infty, \tag{30}$$

which has solutions when the denominator is zero

$$n^2 = P \qquad n^2 = \frac{RL}{S}. \tag{31}$$

The dispersion relation for the ordinary mode (O-mode) emerges from the solution $n^2 = P$. By inserting the definition of P from Eq. (24) and with the assumption $\omega_{pi} \ll \omega_{pe}$

$$n^2 = 1 - \sum_s \frac{\omega_{ps}^2}{\omega^2} \approx 1 - \frac{\omega_{pe}^2}{\omega^2}, \tag{32}$$

which is equal to the dispersion of the nonmagnetized plasma. The wave equation Eq. (26) is simplified to

$$\begin{bmatrix} S & -iD & 0 \\ iD & S-P & 0 \\ 0 & 0 & 0 \end{bmatrix} \begin{bmatrix} Ex \\ Ey \\ Ez \end{bmatrix} = 0, \tag{33}$$

which has an eigenvector $\mathbf{E} = (0, 0, Ez)$. For an ordinary mode wave, the electric field is parallel to the external magnetic field, which therefore has no effect on the propagation of the wave.

The solution $n^2 = RL/S$ of Eq. (30) leads to extraordinary waves, which obey the dispersion relation [2]

$$n^2 = 1 - \frac{\omega_{pe}^2}{\omega^2} \frac{\omega^2 - \omega_{pe}^2}{\omega^2 - (\omega_{pe}^2 + \omega_{ce}^2)}. \tag{34}$$

The extraordinary mode (X-mode) has two cut-off frequencies and resonance frequencies. In this assignment the focus lies on the upper X-mode. The polarization of the X-mode can be derived from the wave equation Eq. (26). The resulting eigenvector $\mathbf{E} = (\frac{iD}{S}E_0, E_0, 0)$ shows that the electric field of the X-mode is elliptically polarized perpendicular to the external magnetic field and the magnetic field of the wave is parallel to the external magnetic field.

The dispersion relations for O-mode and X-mode are shown in Fig. 2. The theoretical dispersion for the X-mode is calculated by solving Eq. (34) for ω. Two possible roots exist

$$\omega^2 = \frac{k^2c^2 + 2\omega_{pe}^2 + \omega_{ce}^2}{2} \pm \frac{\sqrt{(k^2c^2 + 2\omega_{pe}^2 + \omega_{ce}^2)^2 - 4(\omega_{pe}^2 + \omega_{ce}^2)(k^2c^2 + \omega_{pe}^4)}}{2}, \tag{35}$$

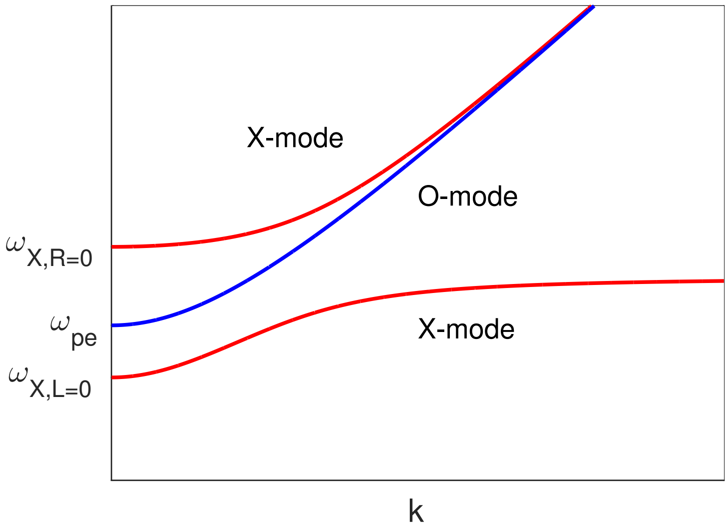

Figure 2: The analytical solution of the dispersion of O-mode given by Eq. (32). The dispersion of the upper X-mode and the lower X-mode are given by Eq. (35). The cut-off frequencies of the X-mode mode waves can be found by setting $n^2 = 0$ in Eq. (34).

where the positive root represents the upper X-mode, and the negative root represents the lower X-mode, both shown in Fig. 2.

2.6 Absorbing boundary

Limited memory provides a challenge for all numerical simulations. Due to the finite size of the simulation region, the boundaries are in a critical role in the realization of the simulation. Especially for the simulation of EM-waves, where in a timescales relevant for the particles of the simulation, the wave has already traversed through the entire simulation region. Ideally waves that reach the edge of the simulation region will disappear from the simulation grid, identical to waves travelling in free space.

For an electromagnetic wave to pass through a boundary without reflection, the electric field components and the derivatives of the electric field components have to be continuous at the boundary. The following derivation of the absorbing boundary conditions closely follows the derivation presented in article [5]. Each component of the electric field independently satisfies the three-dimensional scalar wave equation [6]

$$(\partial_x^2 + \partial_y^2 + \partial_z^2 - c^{-2}\partial_t^2)\mathbf{E} = 0, \tag{36}$$

where $c = c_0/\sqrt{\epsilon\mu}$ is the speed of light in a medium. Solutions of the wave equation depend on place and time as $\mathbf{E} = \mathbf{E}(\mathbf{k} \cdot \mathbf{r} + \omega t)$. The frequency of the wave can be defined with the wave vector as $\omega = kv$, where v is the velocity of the wave. The electric field can be modified to be

$$\mathbf{E}(\mathbf{k}\cdot\mathbf{r}+\omega t)=\mathbf{E}\left(\frac{\omega}{v}\hat{\mathbf{k}}\cdot\mathbf{r}+\omega t\right), \tag{37}$$

where the unit wave vector $\hat{\mathbf{k}}$ is parallel to the velocity of the wave $\hat{\mathbf{k}} \parallel \mathbf{v}$, which allows expressing the components of the unit wave vector as $k_x = v_x/v$, and transforming the argument into

$$\mathbf{E}\left(\omega\left(\frac{v_x}{v^2}x+\frac{v_y}{v^2}y+\frac{v_z}{v^2}z+t\right)\right). \tag{38}$$

With the assumption of constant frequency ω, the argument of the electric field is simplified to

$$\mathbf{E}\left(s_x x+s_y y+s_z z+t\right), \tag{39}$$

where the $s_x = v_x/v^2$ denotes an inverse velocity component. The inverse velocity components satisfy $s_x^2+s_y^2+s_z^2=c^{-2}$. A plane wave traversing to the direction of decreasing x can be modified to

$$\mathbf{E}=\mathbf{E}(t+(c^{-2}-s_y^2-s_z^2)^{1/2}x+s_y y+s_z z)). \tag{40}$$

The first order boundary condition that produces zero reflection coefficient at the boundary located at $x=0$ is[5]

$$(\partial_x - s_x\partial_t)\mathbf{E}|_{x=0}=(\partial_x - c^{-1}(1-(cs_y)^2-(cs_z)^2)^{1/2}\partial_t)\mathbf{E}|_{x=0}=0. \tag{41}$$

The square root of Eq. (41) can be approximated as

$$(1-(cs_y)^2-(cs_z)^2)^{1/2})=1+\mathcal{O}((cs_y)^2+(cs_z)^2), \tag{42}$$

which results in the first order approximation

$$(\partial_x - c^{-1}\partial_t)\mathbf{E}|_{x=0}=0. \tag{43}$$

In its simplest form, the first order boundary condition simply states that the for a wave that approaches the boundary parallel to the normal of the surface, the change of the wave in time has to equal the change in space. A more precise approximation can be achieved if the square root is written as

$$(1-(cs_y)^2-(cs_z)^2)^{1/2})=1-\frac{1}{2}((cs_y)^2+(cs_z)^2+\mathcal{O}(((cs_y)^2+(cs_z)^2)^2), \tag{44}$$

which results in a second order approximation

$$(c^{-1}\partial_{xt}^2-c^{-2}\partial_t^2+\frac{1}{2}(\partial_y^2+\partial_z^2))\mathbf{E}|_{x=0}=0. \tag{45}$$

The second order approximation is also able to absorb a wave that propagates parallel to the border, by incorporating the derivatives of y and z.

2.7 Replacing particles with relative permittivity

Currently the MULTI-em simulation is fully kinetic, which is computationally expensive and limits the possible targets for the simulation. The effect of the particle currents on the propagation of the EM-waves enters the simulation in Eq. (61) in the current term. If this current term could be replaced with an analytical formula, particles could be left out of the simulation.

For isotropic plasma, the current is already given as a function of the electric field and conductivity tensor in Eq. (15). The imaginary part can be gotten rid of by assuming harmonic time dependencies into a another direction $-i\omega\mathbf{E} = \partial\mathbf{E}/\partial t$ and remembering the definition of plasma frequency $\omega_p^2 = ne^2/m\epsilon_0$ the current can be denoted with

$$\mathbf{J} = \frac{ie^2 n_e}{m_e\omega}\mathbf{E} = \epsilon_0 \frac{\omega_{pe}^2}{\omega^2}\frac{\partial\mathbf{E}}{\partial t}. \tag{46}$$

By replacing the current term in the amperé's law used to calculate the propagation of the electric field in the simulation Eq. (61)

$$\frac{\partial\mathbf{E}}{\partial t} = \frac{1}{\epsilon_0}\nabla\times\mathbf{H} - \frac{\mathbf{J}}{\epsilon_0} = \frac{1}{\epsilon_0}\nabla\times\mathbf{H} - \frac{\omega_{pe}^2}{\omega^2}\frac{\partial\mathbf{E}}{\partial t}, \tag{47}$$

which can be simplified by taking the electric field derivative as a common divisor

$$\frac{\partial\mathbf{E}}{\partial t} = \left(1 - \frac{\omega_{pe}^2}{\omega^2}\right)^{-1}\frac{1}{\epsilon_0}\nabla\times\mathbf{H}. \tag{48}$$

The factor can be denoted as a relative permittivity $\epsilon_r = (1 - \omega_{pe}^2/\omega^2)$ and $\epsilon = \epsilon_r\epsilon_0$, which results in a final simple formulation for the derivative of the electric field

$$\frac{\partial\mathbf{E}}{\partial t} = \frac{1}{\epsilon}\nabla\times\mathbf{H}, \tag{49}$$

Without external magnetic field, when the frequency of the EM-wave is close to the plasma frequency, the wave is transient and unable to propagate. The Eq. (49) approaches infinity close to the plasma frequency, which makes the application of the equations to the MULTI-em simulation more complicated.

For plasma with an external magnetic field, the current can be calculated from the electric field with a second order conductivity tensor. The current term is shown in Eq. (22). The effect of the ions on the current is neglected for now and can be introduced later with a simple addition. The choice of the direction of the external magnetic field is arbitrary, here the magnetic field is in z-direction $\mathbf{B}_0 = B_0\hat{\mathbf{z}}$. The brackets can be opened to produce three equations for the components of the current

$$J_x = \epsilon_0 \omega_{pe}^2 \left(\frac{-i\omega}{\omega_{ce}^2 - \omega^2} E_x + \frac{\omega_{ce}}{\omega_{ce}^2 - \omega^2} E_y \right) \tag{50}$$

$$J_y = \epsilon_0 \omega_{pe}^2 \left(\frac{-\omega_{ce}}{\omega_{ce}^2 - \omega^2} E_x + \frac{-i\omega}{\omega_{ce}^2 - \omega^2} E_y \right) \tag{51}$$

$$J_z = \epsilon_0 \omega_{pe}^2 \left(\frac{i}{\omega} E_z \right). \tag{52}$$

The assumption of harmonic time-dependencies $-i\omega\mathbf{E} = \partial\mathbf{E}/\partial t$, can be used to transform the imaginary parts into to a form that easier to implement

$$J_x = \epsilon_0 \left(\frac{\omega_{pe}^2}{\omega_{ce}^2 - \omega^2} \frac{\partial E_x}{\partial t} + \frac{\omega_{ce}}{\omega_{ce}^2 - \omega^2} E_y \right) \tag{53}$$

$$J_y = \epsilon_0 \left(\frac{\omega_{pe}^2}{\omega_{ce}^2 - \omega^2} \frac{\partial E_y}{\partial t} - \frac{\omega_{ce}}{\omega_{ce}^2 - \omega^2} E_x \right) \tag{54}$$

$$J_z = -\epsilon_0 \left(\frac{\omega_{pe}^2}{\omega^2} \frac{\partial E_z}{\partial t} \right). \tag{55}$$

The electric field for E_x according to Eq. (61) is now

$$\frac{\partial E_x}{\partial t} = \frac{1}{\epsilon_0} \left(\frac{\partial H_z}{\partial y} - \frac{\partial H_y}{\partial z} \right) - \left(\frac{\omega_{pe}^2}{\omega_{ce}^2 - \omega^2} \frac{\partial E_x}{\partial t} + \frac{\omega_{ce}}{\omega_{ce}^2 - \omega^2} E_y \right), \tag{56}$$

where the electric field time derivative can be taken as a common denominator, which results in

$$\frac{\partial E_x}{\partial t} = \left(1 + \frac{\omega_{pe}^2}{\omega_{ce}^2 - \omega^2} \right)^{-1} \frac{1}{\epsilon_0} \left(\frac{\partial H_z}{\partial y} - \frac{\partial H_y}{\partial z} \right) - \left(\frac{\omega_{ce}}{\omega_{ce}^2 - \omega^2} E_y \right) \tag{57}$$

$$\frac{\partial E_y}{\partial t} = \left(1 + \frac{\omega_{pe}^2}{\omega_{ce}^2 - \omega^2} \right)^{-1} \frac{1}{\epsilon_0} \left(\frac{\partial H_x}{\partial z} - \frac{\partial H_z}{\partial x} \right) + \left(\frac{\omega_{ce}}{\omega_{ce}^2 - \omega^2} E_x \right) \tag{58}$$

$$\frac{\partial E_z}{\partial t} = \left(1 - \frac{\omega_{pe}^2}{\omega^2} \right)^{-1} \frac{1}{\epsilon_0} \left(\frac{\partial H_y}{\partial x} - \frac{\partial H_x}{\partial y} \right) \tag{59}$$

In the absence of an external magnetic field $\omega_{ce} = 0$, which reduces Eq. (57) to the same as in the isotropic case. These solutions assume that there in fact exists a propagating wave with a certain frequency. Different approaches and the implementation of dispersive media in a FDTD-simulation are described by Taflove [7], Luebbers in [8], and [9].

3 Research material and methods

3.1 Description of the MULTI-em simulation

The simulation platform used is based on a hybrid plasma simulation platform that has been developed to study planetary plasma environments. The addition of electromagnetic waves was done by Pohjola and Kallio [10] to create a fully–kinetic electromagnetic simulation–platform.

The simulation treats both electrons and ions as fully kinetic particles. The particles are implemented as macroparticles, which represent millions of actual particles. The simulation uses a FDTD-method to propagate both electric and magnetic fields. The magnetic field is propagated in time by using the Faraday's law Eq. (7)

$$\frac{\partial \mathbf{B}}{\partial t} = -\nabla \times \mathbf{E}. \tag{60}$$

The electric field is propagated in time by using the Ampère-Maxwell's law Eq. (8)

$$\frac{\partial \mathbf{E}}{\partial t} = \frac{1}{\epsilon_0}\nabla \times \mathbf{H} - \frac{\mathbf{J}}{\epsilon_0}, \tag{61}$$

where the electric current is calculated from the bulk velocity of ions and electrons, $\mathbf{u}_s$ and $\mathbf{u}_e$, respectively

$$\mathbf{J} = \sum_s (q_s n_s \mathbf{u}_s) - e n_e \mathbf{u}_e. \tag{62}$$

Macroparticles are accelerated by the Lorentz force Eq. (6). The bulk velocities $\mathbf{u}_s$ and $\mathbf{u}_e$ needed in Eq. (62) are derived by accumulating particles into a cell (see [10] for details). If the the Gauss law for the electric field Eq. (9) and the equation of continuity for charge are satisfied initially

$$\nabla \cdot \mathbf{J} = -\partial \rho / \partial t. \tag{63}$$

Taking the divergence of Eq. (61)

$$\partial(\nabla \cdot \mathbf{E} - \rho \epsilon_0)/\partial t = 0. \tag{64}$$

Eq. (64) implies that if the Gauss' law (Eq. (9)) is fulfilled initially, it will be filled during the simulation, without the need to solve Poisson's equation.

The simulation region consists of cubic grid cells that are surrounded by so called ghost cells, which are used for the calculation of the electric and magnetic fields at the edge of the grid. The electric field values are stored at the cell edges and the magnetic field values at the cell faces, similar to a Yee-type grid shown in Fig. 4. It is possible that the propagation of particles takes them outside the actual simulation region. Currently these particles can either be absorbed or reflected by the boundaries. With a low number of macroparticles in a cell, these escaping particles provide an significant source of instability, especially with an external static magnetic field.

Each grid cell is described with three indexes i, j, and k. The ghost cells correspond to indeces $i = 0, i = nx - 1, j = 0, j = ny - 1, k = 0, k = nz - 1$, where nx, ny, and nz are the numbers of cells in $x, y, \text{and} z$ directions, respectively. Only cell edges and faces of actual grid cells are initialized and reference to an edge or a face outside the actual simulation area will result in a segmentation fault. The edges, cells, and nodes for each cell are referenced through a straight-forward indexing scheme. For each cell, there is a total number of 12 edges.

3.2 Finite-difference time-domain method

Finite-difference time-domain (FDTD) method is one of most frequently used methods in computational electrodynamics. The method was first introduced by Yee in 1966 [3]. The FDTD method does not require solving complicated linear algebra and the error sources are well understood. FDTD method is memory intensive to a point [7].

The FDTD method uses a Yee-type grid shown in Fig. 4. The grid consists of cells where the magnetic field values are saved on the cell faces and electric field values are saved on the cell edges. Maxwell's equations

$$\frac{\partial \mathbf{B}}{\partial t} = -\nabla \times \mathbf{E} \tag{65}$$

$$\mu_0 \epsilon_0 \frac{\partial \mathbf{E}}{\partial t} = \nabla \times \mathbf{B}, \tag{66}$$

allow the calculation of the magnetic field on the face from the electric field values on the edge of the corresponding face. The electric field is calculated at integer time-steps and the magnetic fields are calculated at half-integer time-steps. With a finite-difference approximation the electric and magnetic field x-components are [5]

$$\begin{aligned} H_x^{n+1/2}(i, j+1/2, k+1/2) = H_x^{n-1/2}&(i, j+1/2, k+1/2) \\ -\frac{\delta t}{\mu_0 \delta}&(E_z^n(i, j+1, k+1/2) - E_z^n(i, j, k+1/2) \\ &-E_y^n(i, j+1, k+1) + E_y^n(i, j+1/2, k)), \end{aligned} \tag{67}$$

$$\begin{aligned} E_x^{n+1}(i+1/2, j, k) = E_x^n&(i+1/2, j, k) \\ +\frac{\delta t}{\mu_0 \delta}&(H_z^{n+1/2}(i+1/2, j+1/2, k) - H_z^{n+1/2}(i+1/2, j-1/2, k) \\ &-H_y^{n+1/2}(i+1/2, j, k1/2) + H_y^{n+1/2}(i+1/2, j, k-1/2)), \end{aligned} \tag{68}$$

where δt is the time step of the simulation and δ the length of grid cell edge. The y and z-components are calculated similarly. Calculating new electric(magnetic) field values only requires the value of the previous field value, and the value of magnetic(electric) field value at previous time-step, which allows the simulation to update all the electric(magnetic) field values in parallel.

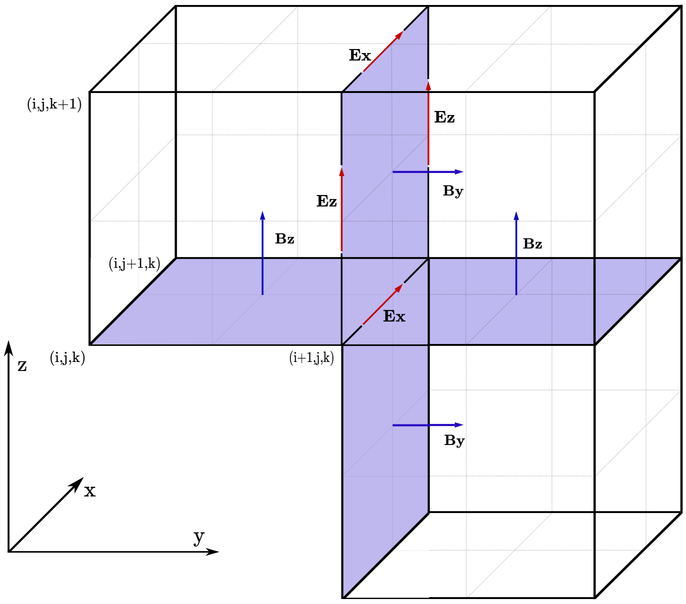

Figure 4: The position of the field components in a Yee-type grid. The magnetic field $B_y(i+1, j+1/2, k+1/2)$ is calculated from the electric field components on the border of the face marked in red. The electric field component $E_x(i+1, j+1/2, k)$ is calculated from the four nearest magnetic field components from the faces marked in blue.

3.3 Absorbing boundary conditions for FDTD

There are two popular possibilities of implementing a boundary for FDTD-simulation that absorbs EM-waves at the boundary. The continuous boundary conditions, where the electric field is calculated at the edge of the grid to create a seemingly continuous wave, and the perfectly matched layer (PML), where a boundary layer with a matching impedance is added. The approach with PML has gained popularity in recent years, but the continuous boundaries are easier to implement, although less precise. PML boundary is more complicated to implement for plasma simulations because of the non-scalar conductivity of magnetized plasma. This section describes the practical implementation of the continuous boundary conditions for a FDTD-simulation. The absorbing boundary conditions for the numerical simulation of waves presented by Enquist and Majda [4] were adapted to the simulation of EM-waves using FDTD-method by Mur [5].

The absorbing boundary conditions are derived analytically in Section 2.6. However, the discrete simulation grid provides an additional difficulty of the realisation of such boundary conditions. For a Yee-type grid shown in Fig. 4, magnetic field components can be evaluated on the edge of the grid from the electric field components on the edge. However, the calculation of the electric field components would require magnetic field components that are located outside of the simulation grid. The idea of these absorbing boundary conditions is to calculate the electric field component at the edge of the grid in such a way that the wave seems to be continuous at the boundary, demonstrated in Fig. 5.

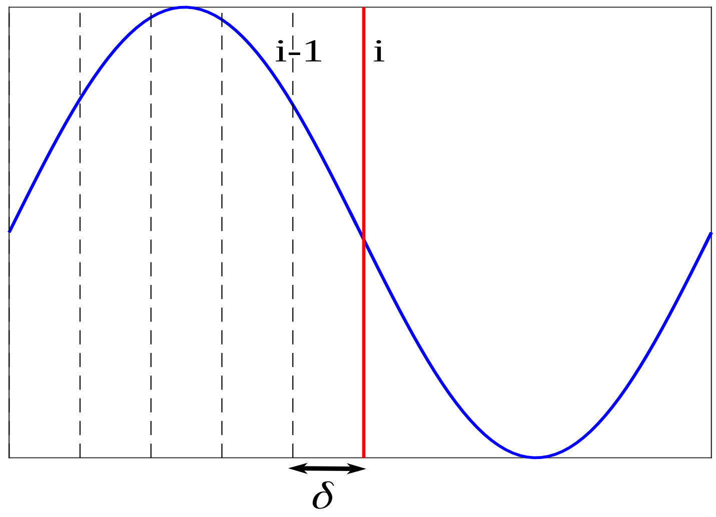

Figure 5: Visualization of the absorbing boundary conditions. The 1D-wave (blue) arrives at the boundary (red) on a discrete grid. The amplitude of the wave is only known at the grid points. The spatial derivative is calculated at a time step t at grid points $i-1$ and i. The time derivative is then calculated at grid point $i-1$ at time steps t and $t+\Delta t$. The amplitude of the wave corresponding to a wave without the boundary is estimated with these derivatives at grid point i at time step $t+\Delta t$.

In the simulation, magnetic–field values are replicated to ghost cells surrounding the actual grid to typical calculation of electric field at the edge. These electric field values at the edge of the grid are replaced by electric field values of an absorbing boundary. The analytical solution of a first approximation Eq. (43) for an electric field at the edge of the grid absorbs the perpendicular component of a wave that arrives to the boundary. The analytical solution can be implemented with a finite-difference approximation. Here the absorbing boundary is calculated for a component $E_z^{n+1}(0, j, k+1/2)$, which denotes electric-field component in z-direction on the 'left' edge of a simulation box at a time-step $n+1$. Indexes j and k are dropped on the following derivation of the first order absorbing boundary. The finite-difference of the electric field at the edge is

$$\begin{aligned} &\frac{1}{\delta}(E_z^{n+1}(1) - E_z^{n+1}(0)) + \frac{1}{\delta}(E_z^{n}(1) - E_z^{n}(0)) \\ -&\frac{1}{c\delta t}(E_z^{n+1}(0) - E_z^{n}(0)) - \frac{1}{c\delta t}(E_z^{n+1}(1) - E_z^{n}(1)) = 0, \end{aligned} \tag{69}$$

where spacial derivatives and time-derivatives are calculated for grid points $(0, j, k+1/2)$ and $(1, j, k+1/2)$ and for times n and $n+1$. The electric field E_z^{n+1} can be solved from Eq. (69)

$$E_z^{n+1}(0) = E_z^n(1) + \frac{c\delta t - \delta}{c\delta t + \delta}(E_z^{n+1}(1) - E_z^n(0)), \tag{70}$$

where the term $E_z^{n+1}(1)$ requires calculation of of the electric field everywhere else except at the boundary.

The second order approximation for an absorbing boundary can be derived from Eq. (45). The derivation is not shown here, but follows the same ideas as the derivation of the first order absorbing boundary. This time the indexes j and k cannot be forgotten. The electric field $E_z^{n+1}(i, j, k + 1/2)$ is solved

$$\begin{aligned}
E_z^{n+1}(0, j, k + 1/2) = & - E_z^{n-1}(1, j, k + 1/2) \\
& + \frac{c\delta t - \delta}{c\delta t + \delta}(E_z^{n+1}(1, j, k + 1/2) + E_z^{n-1}(0, j, k + 1/2)) \\
& + \frac{2\delta}{c\delta t + \delta}(E_z^n(0, j, k + 1/2) + E_z^n(1, j, k + 1/2)) \\
& + \frac{(c\delta t)^2}{2\delta(c\delta t + \delta)}(E_z^n(0, j + 1, k + 1/2) - 2E_z^n(0, j, k + 1/2) \\
& \quad + E_z^n(0, j - 1, k + 1/2) + E_z^n(1, j + 1, k + 1/2) \\
& \quad - 2E_z^n(1, j, k + 1/2) + E_z^n(1, j - 1, k + 1/2) \\
& \quad + E_z^n(0, j, k + 3/2) - 2E_z^n(0, j, k + 1/2) \\
& \quad + E_z^n(0, j, k - 1/2) + E_z^n(1, j, k + 3/2) \\
& \quad - 2E_z^n(1, j, k + 1/2) + E_z^n(1, j, k - 1/2)).
\end{aligned} \tag{71}$$

The electric field components needed to calculate the second order approximation are shown in Fig. 6. The second order approximation requires electric-field components from a time-step $n-1$. The implementation of the second order approximation is more complex because of needed adjacent components in all directions. These components do not exist at the edge of the simulation box. However, the components outside of the simulation box can be set to zero. This simply implies that no wave approaches the box from outside.

3.4 Notable differences compared to previous versions

In the previous version of MULTI-em model, electromagnetic waves were produced by either a varying magnetic field or a varying electric field. Using varying magnetic fields as a wave source is not very intuitive and creates problems, when the simulation needs a constant magnetic field. The varying magnetic fields were created through the constant magnetic field functions, which are also used in particle propagation. During this assignment it was decided that all electromagnetic waves will be created by using a varying electric field source.

Previously the electric field values at the source location were overwritten by the forced source field. Therefore, waves travelling towards the source location were not able to pass the source.This is problematic, especially with plane wave sources that have equal width with the simulation box and thus prevent reflected waves from escaping the simulation box on the side of the source. The problem was alleviated by adding a different variable for a forced electric field source. The change of the magnetic field is calculated as the curl of the normal electric field and the source electric field

$$\frac{\partial \mathbf{B}}{\partial t} = -\nabla \times (\mathbf{E} + \mathbf{E}_{source}). \tag{72}$$

Multiple new electromagnetic wave sources were added, most notable being an elliptically polarized point source called "sinEPolarized", which takes phase difference between E_y and E_z as a parameter.

The electric field was previously interpolated from cell edges to cell nodes for the propagation of the magnetic field. The magnetic field is now calculated directly from the electric field values at the edges of the cells. Previously, the electric field was interpolated from cell nodes to cell center for particle propagation. Now, the electric field is interpolated directly from the cell edges to the cell center. The electric field x-component at the cell center is calculated as the mean of the electric field values of the cell's four edges in x-direction. In total, all 12 cell edges are used for the interpolation of every electric field calThe $ttothecellcenter.y$ and z-comcomponenponents of the electric field are calculated in the same manner, The cell edges now have a location coordinate and resistivity η, which can be used to implement relative permittivity according to a predetermined resistivity profile.

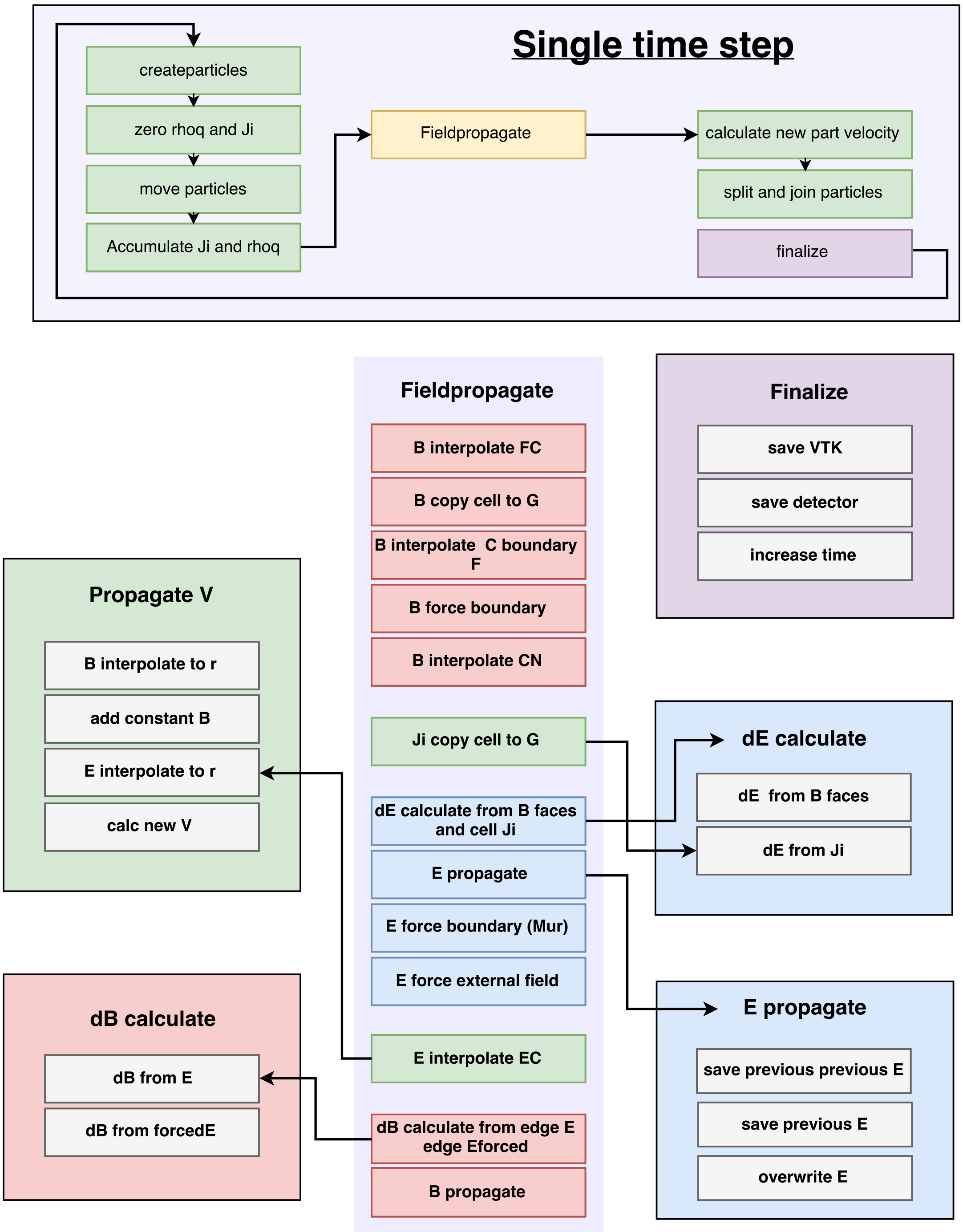

Figure 3: Illustration of a single simulation time step. The green, red, and blue color boxes correspond to functions that are connected to particles, the magnetic field, or the electric field, respectively. The upper part of the figure represents the higher level structure of one time step. The steps that propagate the fields, calculate new particle velocities, and finalize the time step are opened in more detail. Some of the more complex operations have a further description in their own boxes. Boxes below the *Fieldpropagate* correspond to operations that are needed to propagate the electric and magnetic fields one time step forward. Arrows starting from these operations represent a function call required to perform that operation. Most of the boxes have a function call with a similar name in the actual simulation. EC, FC, and CN are short hands for different interpolations (see abbreviations).

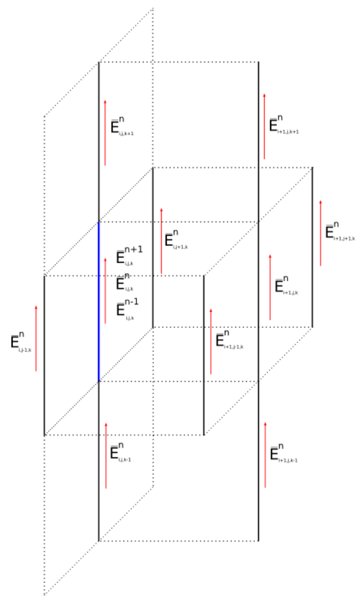

Figure 6: The illustration of the Electric field components that have an effect on the boundary conditions. The Electric field calculated at the edge (blue line) is calculated from all other edges.

4 Results

4.1 Absorbing boundary conditions

To be able to calculate the finite-differences of the electric field components at the edge of the grid, the electric field components of the previous time-step have to be saved. The second approximation of the absorbing boundary conditions requires saving the electric field values at two previous time-steps.

The second order boundary conditions are implemented for the simulation. A final implementation requires the addition of the cell edges to the ghost cells for the calculation of the electric field components at the edge of the simulation box. Currently the components at the edge of the simulation are calculated using the first order approximation for the absorbing boundaries, which only absorb wave that propagate perpendicular to the boundary. The contour lines of the electric field of a a point source E_z located at $\{x, y\} = \{-100, 100\}$ km are shown in Fig. 7. For reference, the countour lines without absorbing boundaries are shown in Fig. A1.

The second order boundary conditions retain the waveform of a point source located close the the corner of the simulation box. The largest differences from the analytical radiation pattern, which is circular, can be seen close to the edges of the simulation box.

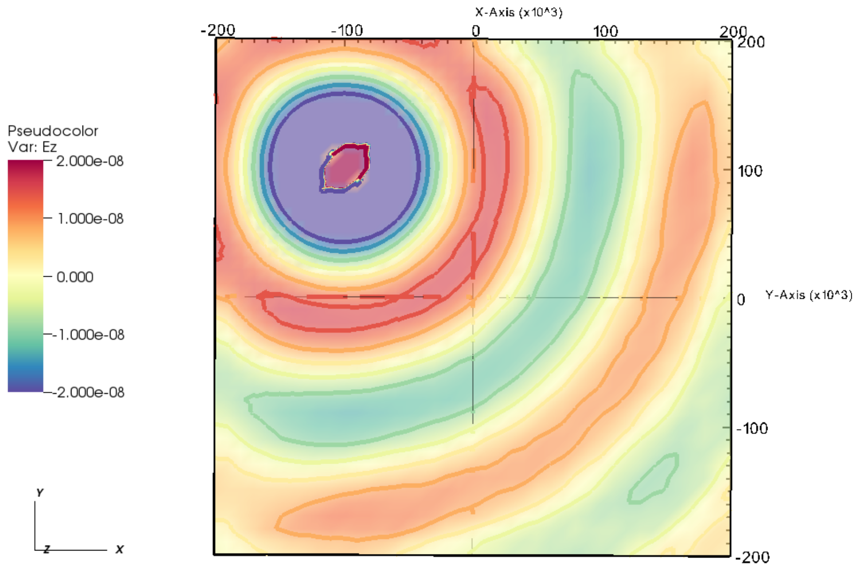

Figure 7: The contour lines of the EM-wave produced by a point source E_Thez with $f = 2000$ Hz located at $\{x, y\} = \{-100, 100\}$ km shown at a time $t = 0.0023$ s. size of the simulation box is 400km $\times$ 400km $\times$ 100km. Electric field components at all edges are calculated using the second order approximation Eq. (71)

4.2 Dispersion in nonmagnetized plasma

In plasma, the wavelength and frequency are connected through a nonlinear dispersion relation. In the simulation, the propagation of EM-waves is not artificially restricted.

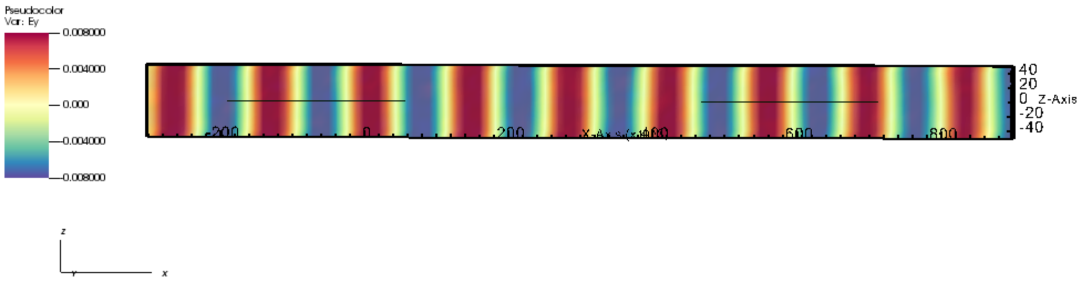

Figure 8: A test of the propagation of a plane wave in nonmagnetized plasma. The color gives the magnitude of the electric field y-component in V/m. A plane wave source of is located at $x = 0$ with a frequency of $f = 2500$ Hz. The entire simulation box if filled with a uniform plasma with plasma frequency of $f_{pe} = 1300$ Hz. The size of the simulation box is 1000 km×100 km×100 km.

The propagation of the wave is only affected through the current term in the Amperè's law Eq. (8), which is calculated from the movement of the macroparticles. The appearance of dispersive characteristics in this fully kinetic simulation is a solid validation for the simulation platform.

The dispersion in isotropic plasma is studied with a plane wave. The plane wave is produced by manually changing the E_y components of the electric field at the plane $x = 0$, which results in a magnetic field component B_z. The width of a single cell is 10 km and the size of the entire grid is $1000 \times 100 \times 100$ km. The electric field source-components are varied with frequencies from 1200 Hz to 2500 Hz. The amplitude of electric–field source is 0.01 V/m. The amplitude of the plane–wave source has no effect on the waveform on tested amplitude range of $E = 1 \cdot 10^{-7} - 1 \cdot 10^{0}$ V/m. The wavelength of the highest frequency $f = 2500$ Hz in vacuum is 120 km, which results in 12 cells for each wavelength at minimum. The simulation time-step $\delta t = 1 \cdot 10^{-5}$ is selected to fill the Courant stability-condition for a FDTD simulation [7]. The simulation configuration is shown in Fig. 8

Electric and magnetic field values measured at $x = 500$ km are shown in Fig. 9. The oscillation reaches a steady state after an initial phase. The possible reflections from the back wall of the simulation box return to the measurement point at $t = 0.0104$ s at the earliest. The small decrease in the amplitude of the electric field near $t = 0.014$ s could be caused by reflections of the initial wave. Without an external magnetic field, electric field components E_x and E_z are are unexpected and could be attributed to the limited macroparticle count. With a low number of macroparticles local variations in the electron density are expected and may produce local electric field gradients, currents, and magnetic fields.

The accurate frequency of the EM-wave in plasma is calculated from the time-series of the fields, shown in Fig. 9. The frequency amplitude spectrum is calculated with a Fourier transform of the time-series of the electric field component E_y. Amplitude spectrum for a source frequency 1700 Hz is shown in Fig. 10a. A longer time-series would produce a more accurate frequency spectrum, but longer simulation runs face

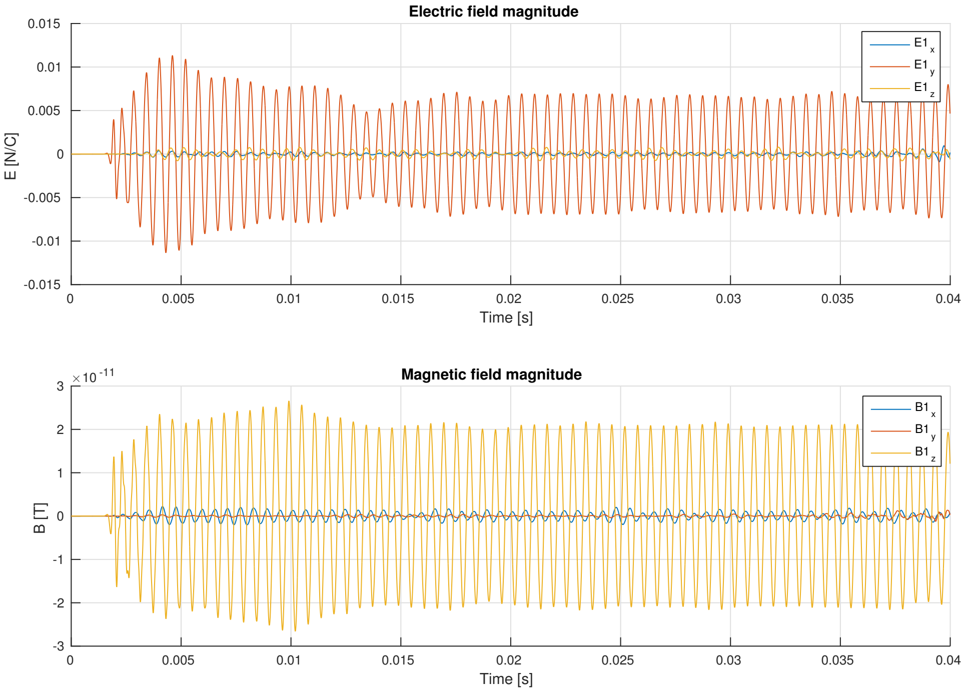

Figure 9: The time-series of electric and magnetic field component amplitudes of a plane wave source in isotropic plasma. The source electric field has magnitude of $E_y = 0.01$ V/m and a frequency of 1700 Hz. The field values are measured at $x = 500$ km.

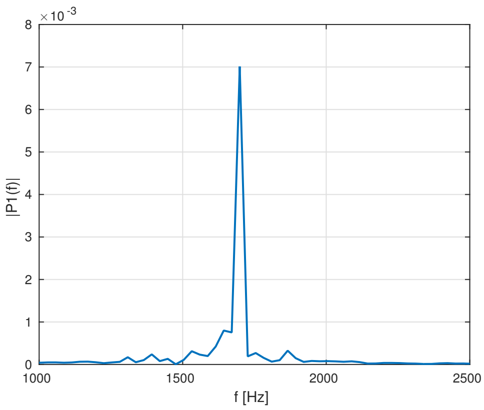

(a) Fourier transform of electric field component E_y for a wave source with frequency $f = 1700$ Hz. The peak is located at frequency $f = 1699$ Hz.

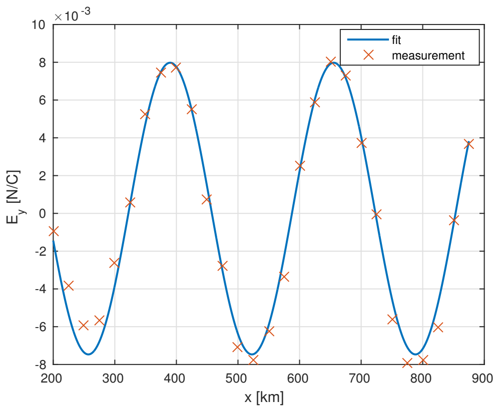

(b) Least-square fit of a function $A\sin(kx + \phi)$ to E_y as a function of position at $t = 0.012$ s.

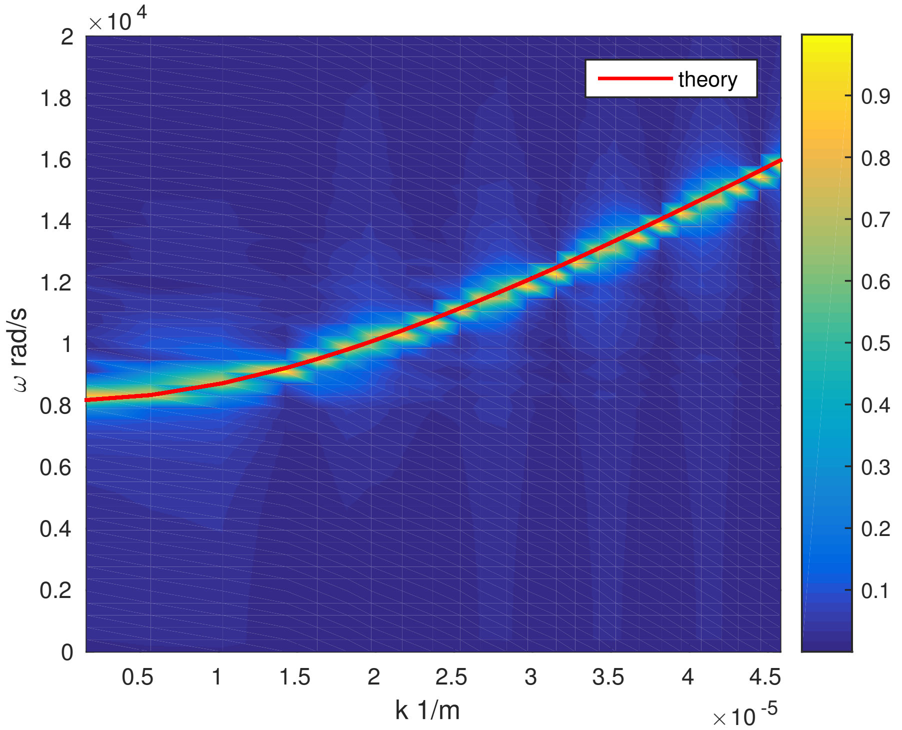

Figure 11: The normalized amplitude spectrum of the electric field as a function of the extracted wave vector k, compared to the theoretical dispersion in cold nonmagnetized plasma. The plasma frequency is $f_{\mathrm{pe}} = 1300$ Hz which corresponds to an angular cut-off frequency of $\omega_{\mathrm{pe}} = 0.82 \cdot 10^4$ rad/s. Amplitude spectrum is obtained with a fast Fourier transform in *Matlab*. See Wiki-page for the analysis code [11].

problems of instability.

The value of the wave vector $k = 2\pi/\lambda$ is obtained from a sinusoidal least-square fit $E_y = A \cdot \sin(kx + \phi)$ to the amplitudes of the electric field component E_y between $200 < x < 875$ km at one moment of time $t = 1200$ s. The least-square fit is shown in Fig. 10b. The frequency amplitude spectrum and value of the corresponding value of k are calculated for multiple source frequencies from 1200 Hz to 2500 Hz. The final result is compiled into a single dispersion relation shown in Fig. 11. The frequency amplitude spectra are obtained from a time-series which ends at $t = 0.02$ s, only half of which is shown in Fig. 9.

The extracted dispersion relation is the compared to the theoretic dispersion calculated using the Eq. (20). The simulation is able to correctly predict the cut-off frequency for an EM-wave in isotropic plasma. Figure 11 demostrates that the simulation is able to describe the nonlinear dispersion of electromagnetic waves in isotropic plasma and to describe the propagation of electromagnetic waves in a nonmagnetized collisionless cold plasma.

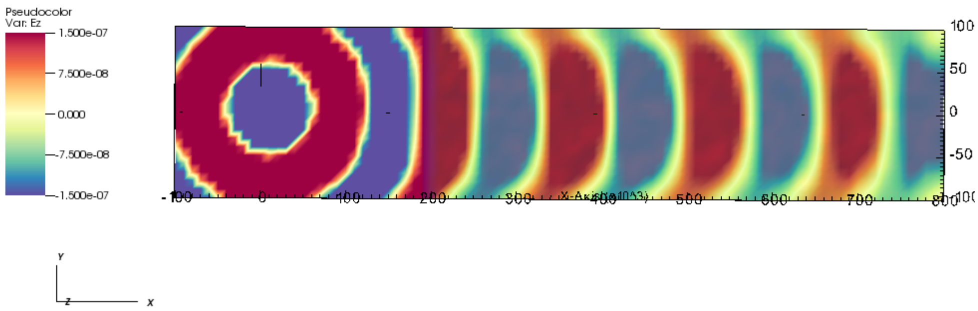

Figure 12: A test of the propagation of the O-wave. The color gives the amplitude of the electric field z-component in V/m. The wave is produced by an oscillating point source at $(x, y, z) = (0, 0, 0)$. The wave source has an electric field amplitude of $E_z = 1 \cdot 10^{-7}$ V/m and a frequency of $f = 2500$ Hz. The external magnetic field $B_z = 40$ nT is in z-direction. The region $x > 200$ is filled with a uniform plasma with a plasma frequency of $f_{pe} = 1300$ Hz. The size of the simulation box is 900 km×200 km×200 km. All boundaries have absorbing boundary conditions for electric fields.

4.3 Dispersion of the O-mode

The O-mode wave has an electric field parallel to the external magnetic field. Charged particles in the plasma oscillate along the external magnetic field, which should therefore not affect the propagation of the wave. For this exact reason, the dispersion of the O-mode is equal to the dispersion of a wave in nonmagnetized plasma Eq. (20). The wave is produced by varying an electric field component E_z on a single edge at the origin $(0, 0, 0)$. An external magnetic field is added to the simulation through a function called "constantMagneticField". The constant magnetic field is ignored in the propagation of the electric and magnetic fields and only affects the propagation of particles. The constant external magnetic field in z-direction $B_{z0} = 40$ nT is applied over the entire simulation box. A uniform plasma region with plasma frequency $f_{\mathrm{pe}} = 1300$ Hz fills the region $x \geq 200$ km. The resulting upper X-mode cut-off frequency is $f_{X,R=0} = 2280$ Hz, lower cut-off frequency is $f_{X,L=0} = 1160$ Hz and the upper resonance frequency $f = 1720$ Hz. The plasma is simulated with 200 macroparticles in a cell.

A single simulation run lasts for $t_{max} = 0.02$ s, and the amplitude of the wave number k is fitted at a time $t = 0.007$ s. The time-series for electric and magnetic fields for multiple frequencies are shown in Figs. A2, A3, A4, and A5. Above the plasma frequency the waveform is clear and close to the source frequency. As the frequency of the incoming wave approaches the X-mode cut-off frequency, the amplitude of high frequency noise increases significantly. At one of the lowest simulated frequencies for the O-mode at $f = 1600$ Hz, the incoming incident wave is quickly damped and is not visible at the end stages of the simulation.

The addition of an external magnetic field has a negative effect on the stability of the simulation. As noted also for the field components in the isotropic simulations,

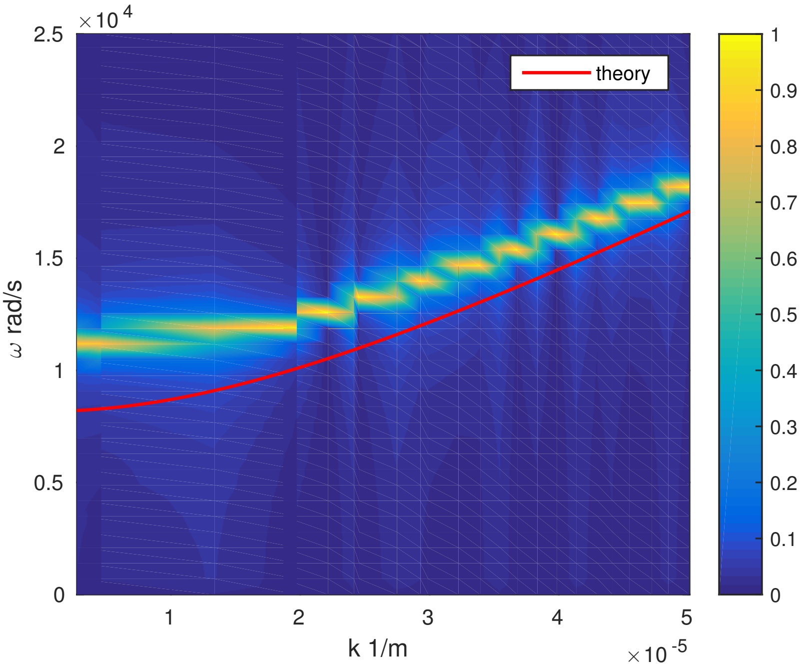

Figure 13: The normalized amplitude spectrum for an O-wave as a function of the extracted k compared to the theoretical dispersion relation of O-mode for cold magnetized plasma. The plasma frequency is $f_{\rm pe} = 1300$ Hz which corresponds to an angular cut-off frequency of $\omega_{\rm pe} = 0.82 \cdot 10^4$ rad/s. The simulated O-mode cut-off is higher at approximately 1750 Hz. Amplitude spectrum is obtained with a fast Fourier transform in *Matlab*. See Wiki-page for the analysis code [11].

unexpected electric and magnetic field components can be seen in Fig. 9. An external magnetic field amplifies the effect of these other components by redirecting particles. The field strengths of a point source are smaller at the edges of the simulation box which alleviates the occurrence of these instabilities. Creating the field with a point source also allows using the absorbing boundary conditions on all edges. Dispersions of the O-mode and X-mode are simulated with a point source.

Largest simulation instabilities arise from the ends of the simulation box. Absorbing boundary conditions in the end of the box result in a situation where particles with same charge are absorbed at the end of the box. This creates a local electric–field gradient, which increases the number of escaping particles over time. The instabilities are attributed to the escaping particles. The electrons do not traverse large distances in comparison the cell size. A larger macroparticle count should decrease the effect of the escaping particles on the total electric field. The effect of increased macroparticle count on the electric fields close to the edge of the simulation box is demonstrated for 40, 120, and 200 macroparticles per cell, shown in Figs. A7, A9, and A11. With a larger number of macroparticles, the absorbtion of a single macroparticle at the end of the box is less significant.

The dispersion relation of the O-mode wave is shown in Fig. 13. The dispersion relation is composed of multiple different simulations similar to the isotropic case. The simulated cut-off frequency of the O-mode is at an frequency $f = 1780$ Hz. The predicted cut-off frequency is the plasma frequency $f_{pe} = 1300$ Hz. The macroparticle count in a cell has little to no effect on the cut-off frequency of the O-mode. This simulated cut-off is close to the upper hybrid resonance frequency of the X-mode. It is important to remember that the plane wave approximation in the derivation of the theoretical dispersion relation is not filled here. The significance of this difference is not investigated further in this assignment.

4.4 Dispersion of upper X-mode

The addition of an external magnetic field introduces new propagating wave modes. When the electric field of the EM-wave is perpendicular to the magnetic field, the charged particles begin oscillating also in the direction of the propagation of the wave and the electric field is expected to be elliptically polarized.

The simulation configuration is shown in Figs. 14a and 14b. A uniform plasma region with plasma frequency $f = 1300$ Hz begins at $x = 200$ km. An external magnetic field $B_z = 40$ nT is applied over the entire simulation box. The resulting upper X-mode cut-off frequency is $f_{X,R=0} = 2280$ Hz, lower cut-off frequency is $f_{X,L=0} = 1160$ Hz and the upper resonance frequency $f = 1720$ Hz. To simulate the dispersion of X-mode, a point source with varying electric field E_y is located at $(0, 0, 0)$. The size of the simulation box is 900 km$\times$200 km$\times$200 km. The addition of external magnetic field introduces new reflections that were not visible in the simulations with nonmagnetized plasma. The resulting asymmetric electric field are clearly visible in Fig. 14b.

The electric and magnetic field time-series is shown in Fig. 15. Even though the original electromagnetic wave has only transverse electric and magnetic fields, upon entering the plasma, the E_x components emerge. This is can be associated with the movement of electrons in x-direction due to the external magnetic field.

In the simulations with external magnetic field, the wave source is not located inside the plasma, because the simulation runs were unstable with a source inside the plasma. A possible reason for this instability could be the acceleration of particles at the source location. The electric field components of E_y have different signs on different sides of the source and particles at the source location experience are not accelerated in a predictable fashion. However, the wave source outside the plasma creates new difficulties with possible shock waves. The electromagnetic waves propagating in the plasma require additional time to reach a stable configuration.

The dispersion of the X-mode is calculated similar to the dispersion relation of nonmagnetized plasma. The frequency amplitude spectrum is obtained as a Fourier transform of the time-series of the electric field component E_y. The corresponding wave number k is extracted by fitting the value of k to E_y at time $t = 0.013$ s. The simulation of the upper X-mode stay stable for a longer time than the simulation of the O-mode. This makes obtaining a cleaner frequency spectrum possible. Even though the electric fields look asymmetric, the extracted dispersion relations are close to the theoretical dispersion of the X-mode. The simulated dispersion relation is shown in Fig. 16.

The dispersion of the upper X-mode displays the same behaviour as the theoretic prediction by Eq. (35). With point source, the frequency spectrum is sharp. As a

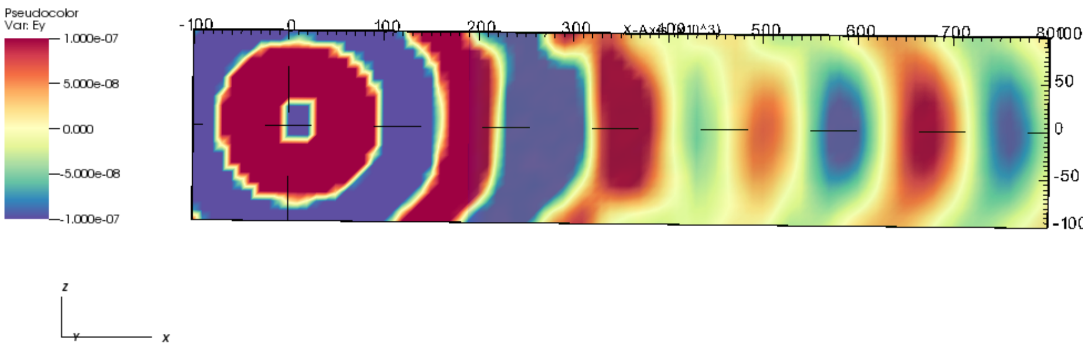

(a) The propagation of the wave in $y = 0$ plane.

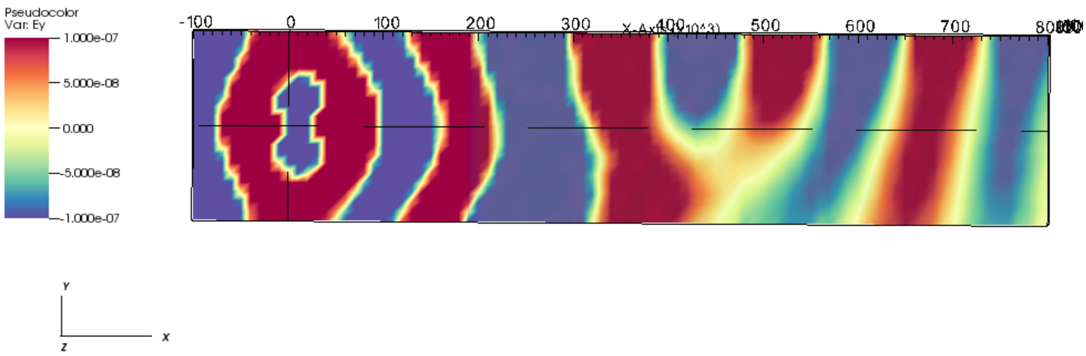

(b) The propagation of the wave in $z = 0$ plane.

Figure 14: A test of the propagation of X-wave in magnetized plasma. The asymmetry of the X-waves is demonstrated by showing the waveform in two different planes. Color gives the amplitude of electric field component E_y. The wave is produced by varying the electric field value on a single edge at $(x, y, z) = (0, 0, 0)$ with an amplitude of $E_y = 1 \cdot 10^{-7}$ V/m. Here, the source frequency is $f = 2500$ Hz. The magnitude of the external magnetic field is $B_z = 40$ nT. A uniform–plasma region with plasma frequency $f_{pe} = 1300$ Hz fills the region $x > 200$ km. The size of the simulation box is 900 km×200 km×200 km.

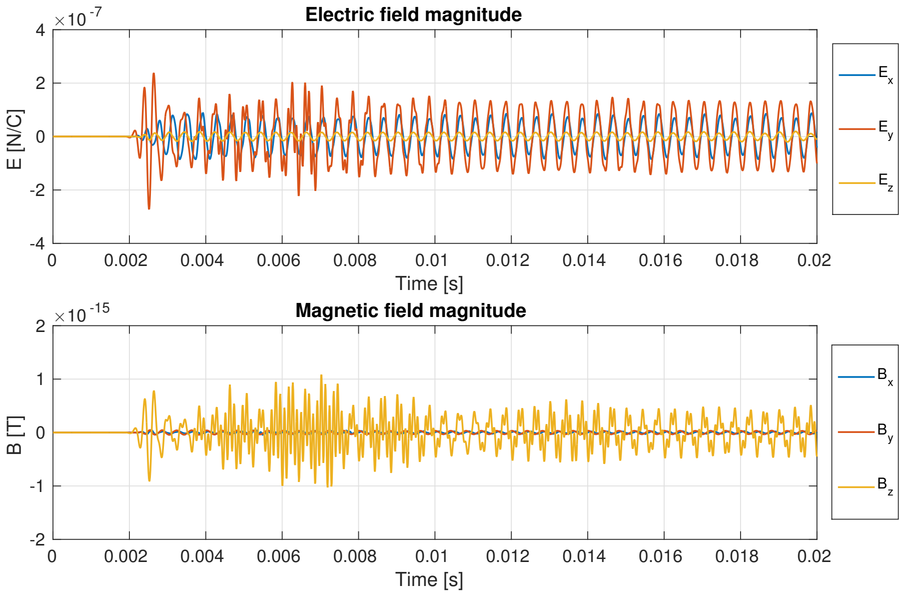

Figure 15: Time-series of the electric and magnetic field components in a test of the propagation of the X-mode. The simulation configuration is shown in Fig. 14b. The EM-wave is produced by an electric field point source located at the origin with an amplitude of $E_y = 1 \cdot 10^{-7}$ V/m and a frequency of $f = 2500$ Hz. The amplitude of the external magnetic field is $B_z = 40$ nT. The fields are measured inside the plasma region at $x = 600$ km.

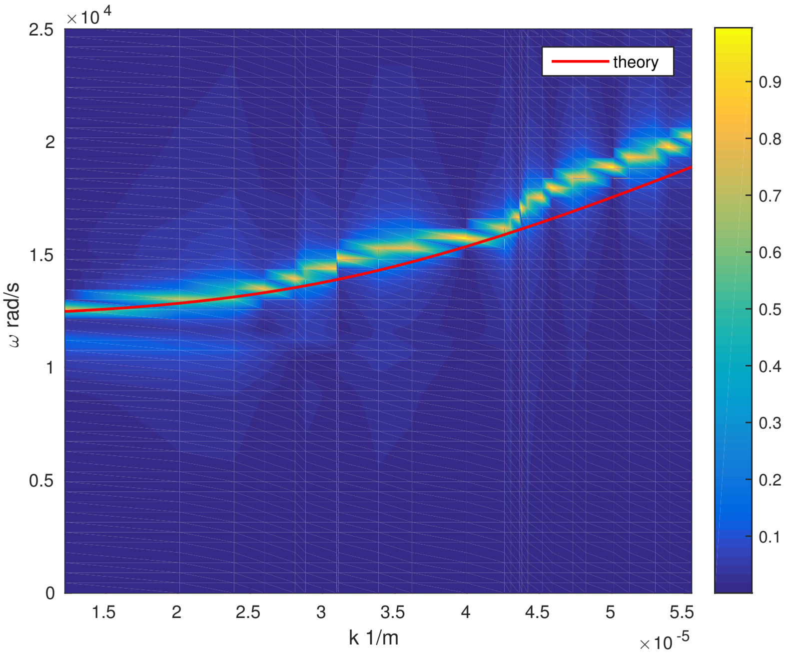

Figure 16: The normalized amplitude spectrum for an O-wave as a function of the extracted k compared to the theoretical dispersion relation of upper X-mode for cold magnetized plasma. The plasma frequency is $f_{\mathrm{pe}} = 1300$ Hz and the upper cut-off frequency $f_{X,R=0} = 2280$ Hz$= 1.4 \cdot 10^4$ rad/s. The simulated upper X-mode cut-off is close to the theoretical cut-off frequency. The simulated dispersion begins to deviate from the theoretical at higher frequencies. Amplitude spectrum is obtained with a fast Fourier transform in *Matlab*. See Wiki-page for the analysis code [11].

result of the fit for the value of k, the obtained values are smaller than predictions made by the theory. The HYB-em seems to be able to correctly predict the nonlinear dispersion of the upper X-mode, the simulated cut-off approaches the cut-off frequency predicted by theory.

The simulation of the lower X-mode was not successful with the current version of the simulation. At lower frequencies the a component of the plasma frequency dominates the frequency spectrum. Also at lower frequencies, the simulation is not as stable as with the higher frequencies. Below the upper X-mode cut-off frequency, it is not possible to obtain a single frequency component from the measured time-series.

5 Summary

This assignment gave an introduction to the fundamental properties of plasma, and the phenomena that are connected to the propagation of an electromagnetic wave in a nonmagnetized and magnetized plasma. The goal of this assignment was the further validation of the HYB-em platform that is based on already validated HYB simulation platform. This goal was approached by investigating the dispersion of electromagnetic waves in different plasma environments. Along the way absorbing boundary conditions were added for electromagnetic waves.

The addition of absorbing boundary conditions allowed a more precise investigation of electromagnetic waves than before. This allowed, for the first time, a reliable investigation of dispersion of EM-waves in plasma with the HYB-em simulation. The dispersion relation for nonmagnetized plasma is in a very good agreement with the theoretical prediction. The dispersion for upper X-mode for magnetized plasma resembles the theoretical prediction with some differences.

Further work includes investigation of the dispersion of the X-mode resonance branch and the dispersion of waves that propagate parallel to the external magnetic field. Important work is required in the reduction of reflections with the addition of external magnetic field and the implementation of stable current boundary conditions.

References

[1] H.G. Booker, Cold Plasma Waves, 1984, p. 1-2.

[2] M.G. Kivelson and C.T. Russell, Introduction to Space Physics, 1995, p. 382

[3] K. Yee, Numerical solution of initial boundary value probles involving Maxwell's equations in isotropic media, *IEEE Transactions on Antennas and Propagation*, Vol. 14, No. 3, pp.302-307, 1966.

[4] B. Encquist and A. Majda, Absorbing boundary conditions for numerical simulation of waves, *Proc. Natl. Acad. Sci. USA*, Vol. 74, No. 5, pp. 1765-1766, 1977.

[5] G. Mur, Absorbing Boundary Conditions for the Finite-Difference Approximation of the Time-Domain Electromagnetic-Field Equations, *IEEE Transactions on electromagnetic compatibility*, vol. 23, No. 4, 1981.

[6] D.J. Griffiths, Introduction to electrodynamics, 1999, p. 368

[7] A. Taflove and S.C. Hagness, Computational Electrodynamics, The Finite-Difference Time-Domain Method, 3rd Edition, 2005

[8] R.J. Luebbers and F. Hunsberger, FDTD for Nth-order dispersive media, *IEEE Transactions on Antennas and Propagation*, Vol. 40, No. 11, 1992.

[9] R.J. Luebbers and K.S. Kunz, A Frequency-Dependent Finite-Difference Time-Domain Formulation for Transient Propagation in plasma, *IEEE Transactions on Antennas and Propagation*, Vol. 39, No. 1, 1991.

[10] V. Pohjola, E. Kallio, On the modeling of planetary plasma environments by a fully kinetic electromagnetic global model HYB-em, *Ann. Geophys.*, Vol. 28,pp. 743-751, doi:10.5194/angeo-28-743-2010, 2010.

[11] The Aalto Wiki-page for internal use. Contains instructions on the running of the simulation and links to the used analysis code, https://wiki.aalto.fi/pages/viewpage.action?title=HYB-em&spaceKey=hybteam, cited 26.4.2017.

A Appendix A

A.1 Countour without absorbing boundary

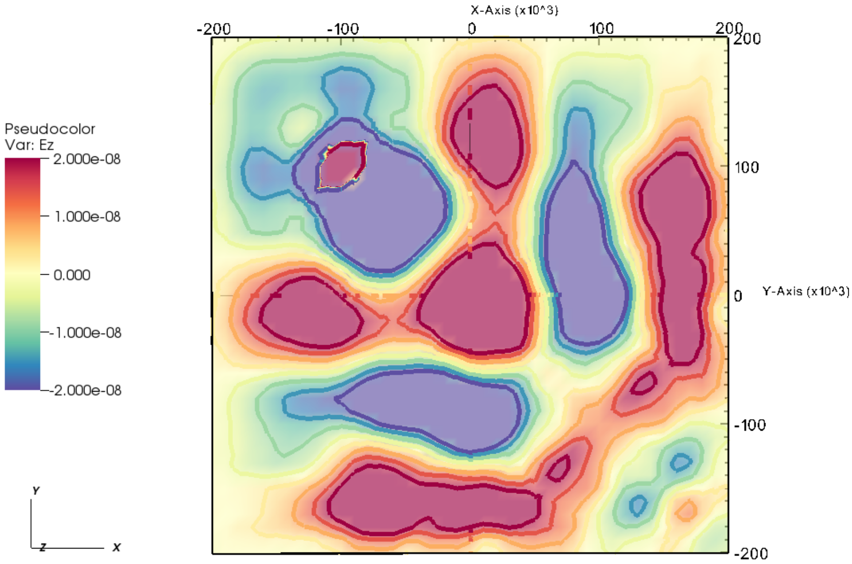

Figure A1: The contour lines of the EM-wave produced by a point source E_z with $f = 2000$ Hz located at $\{x, y\} = \{-100, 100\}$ km shown at a time $t = 0.0023$ s. size of the simulation box is 400km $\times$ 400km $\times$ 100km.

A.2 O-mode fields

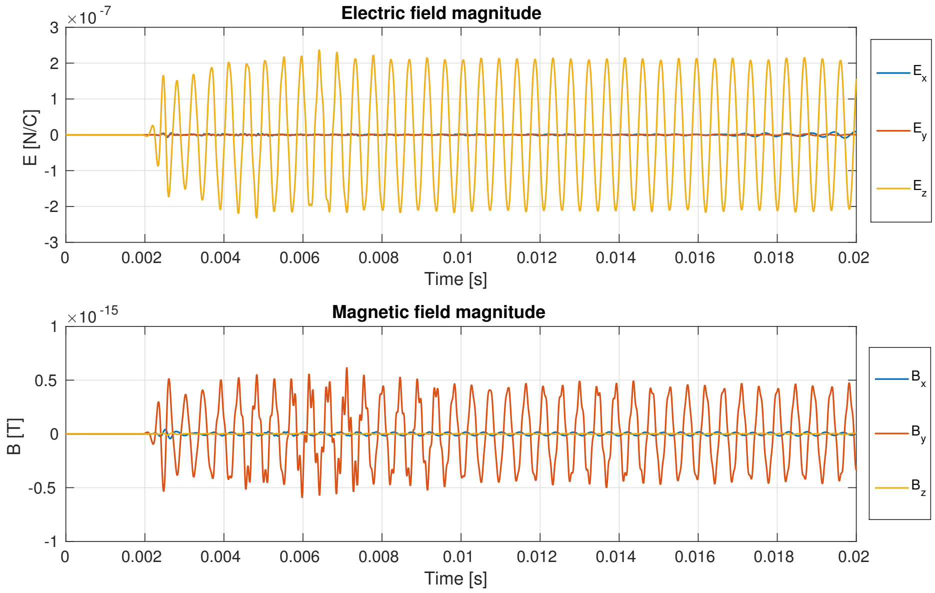

Figure A2: Amplitudes of electric and magnetic field components in a test of the propagation of O-mode. The simulation configuration is shown in Fig. 12. Electric field point source with an amplitude $E_z = 1 \cdot 10^{-7}$ V/m is located at $x = 0$. Amplitude of the external magnetic field is $B_{z0} = 40$ nT. The field amplitudes are measured inside the plasma region at $x = 600$ km for source $f = 2200$ Hz. The plasma frequency is $f_{\mathrm{pe}} = 1300$ Hz.

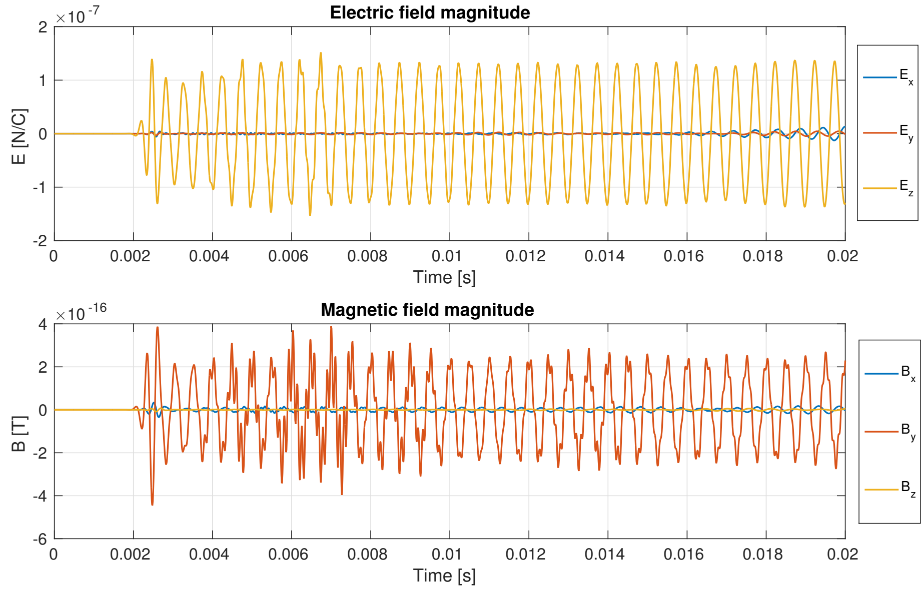

Figure A3: Amplitudes of electric and magnetic field components in a test of the propagation of O-mode. The simulation configuration is shown in Fig. 12. Electric field point source with an amplitude $E_z = 1 \cdot 10^{-7}$ V/m is located at $x = 0$. Amplitude of the external magnetic field is $B_{z0} = 40$ nT. The field amplitudes are measured inside the plasma region at $x = 600$ km for source $f = 2000$ Hz. The plasma frequency is $f_{\rm pe} = 1300$ Hz.

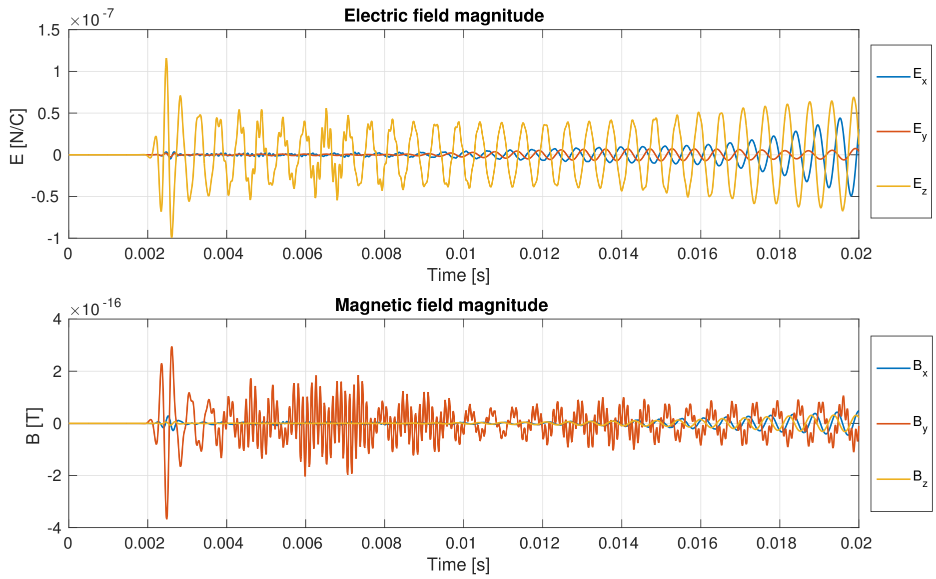

Figure A4: Amplitudes of electric and magnetic field components in a test of the propagation of O-mode. The simulation configuration is shown in Fig. 12. Electric field point source with an amplitude $E_z = 1 \cdot 10^{-7}$ V/m is located at $x = 0$. Amplitude of the external magnetic field is $B_{z0} = 40$ nT. The field amplitudes are measured inside the plasma region at $x = 600$ km for source $f = 1800$ Hz. The plasma frequency is $f_{\rm pe} = 1300$ Hz.

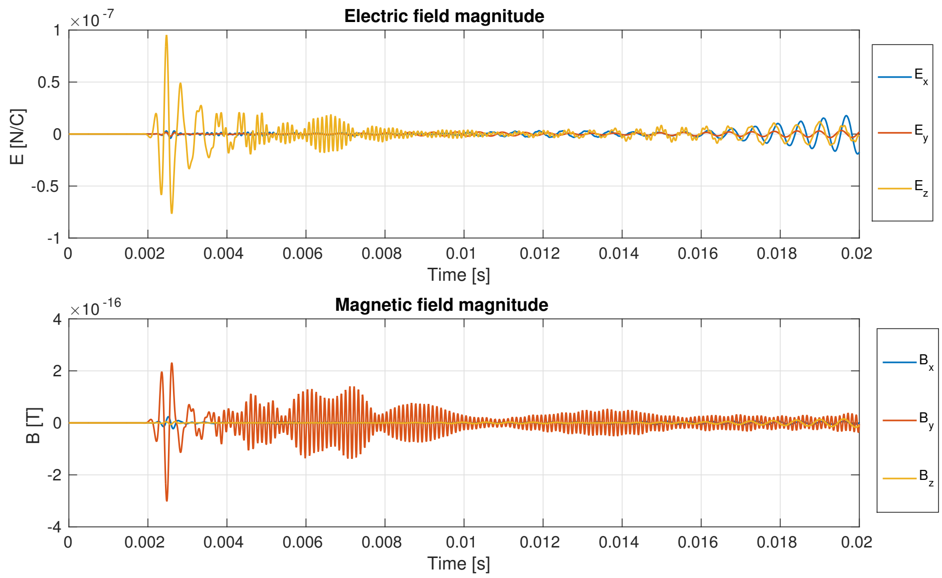

Figure A5: Amplitudes of electric and magnetic field components in a test of the propagation of O-mode. The simulation configuration is shown in Fig. 12. Electric field point source with an amplitude $E_z = 1 \cdot 10^{-7}$ V/m is located at $x = 0$. Amplitude of the external magnetic field is $B_{z0} = 40$ nT. The field amplitudes are measured inside the plasma region at $x = 600$ km for source $f = 1600$ Hz. The plasma frequency is $f_{\rm pe} = 1300$ Hz.

A.3 Effect of macroparticle count on O-mode

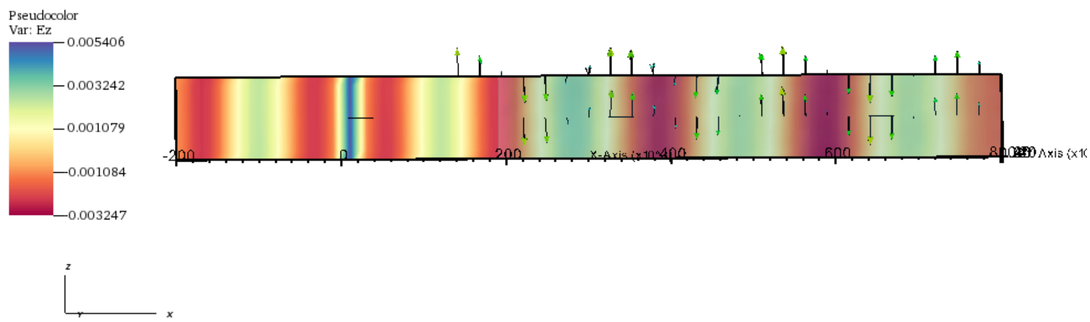

Figure A6: A plane wave source is located at $x = 0$ with a varying electric field E_z at $f = 2200$ Hz and an external magnetic field $B_{z0} = 40$ nT. The simulation box size is $-200 < x < 800$ km and $-50 < y, z < 50$ km. The plasma frequency is $f_{\rm pe} = 1300$ Hz.

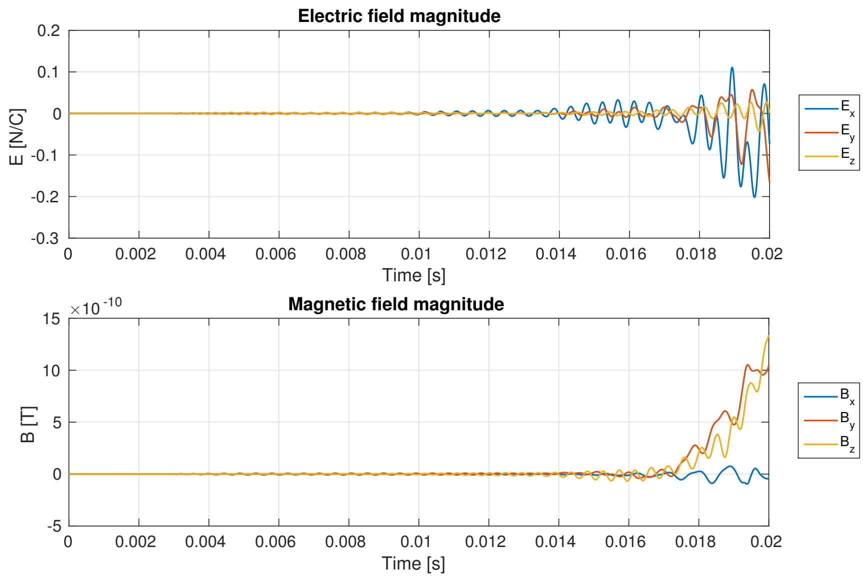

Figure A7: A plane wave source is located at $x = 0$ with a varying electric field E_z at $f = 2200$ Hz and an external magnetic field $B_{z0} = 40$ nT. The plasma frequency is $f_{\text{pe}} = 1300$ Hz. Measured electric and magnetic field values inside the plasma region at $x = 780$ km with 40 macroparticles per cell.

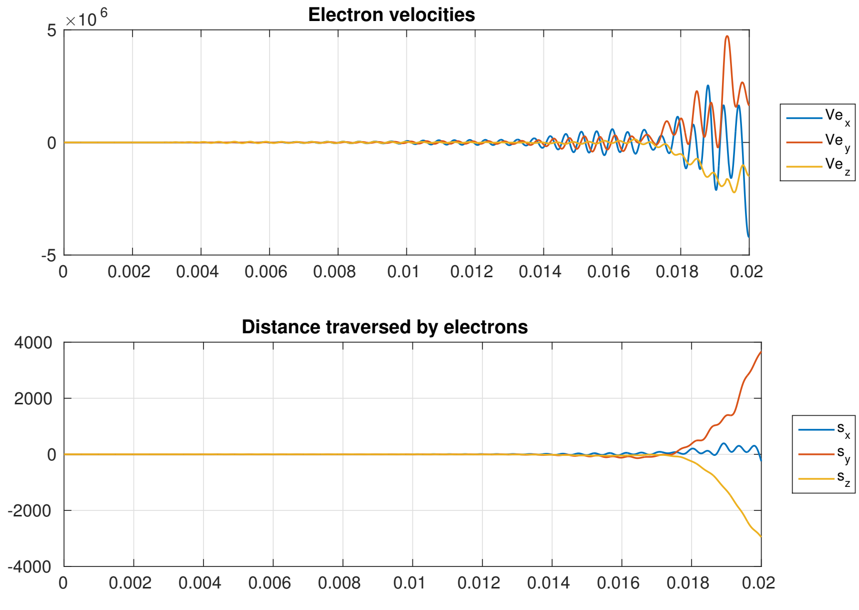

Figure A8: A plane wave source is located at $x = 0$ with a varying electric field E_z at $f = 2200$ Hz and an external magnetic field $B_{z0} = 40$ nT. The plasma frequency is $f_{\text{pe}} = 1300$ Hz. Measured electron velocities inside the plasma region at $x = 780$ km with 40 macroparticles per cell.

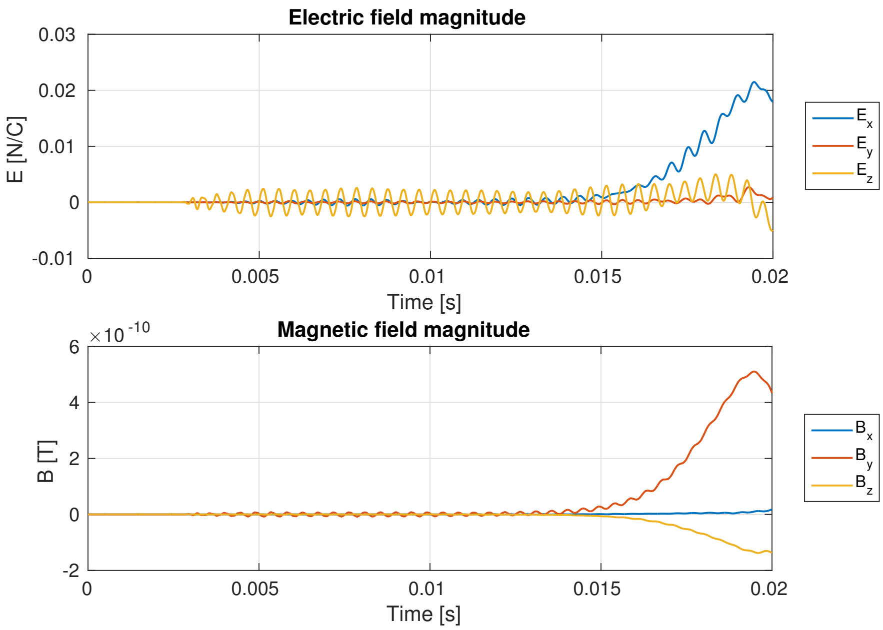

Figure A9: A plane wave source is located at $x = 0$ with a varying electric field E_z at $f = 2200$ Hz and an external magnetic field $B_{z0} = 40$ nT. The plasma frequency is $f_{\mathrm{pe}} = 1300$ Hz. Measured electric and magnetic field values inside the plasma region at $x = 780$ km with 120 macroparticles per cell.

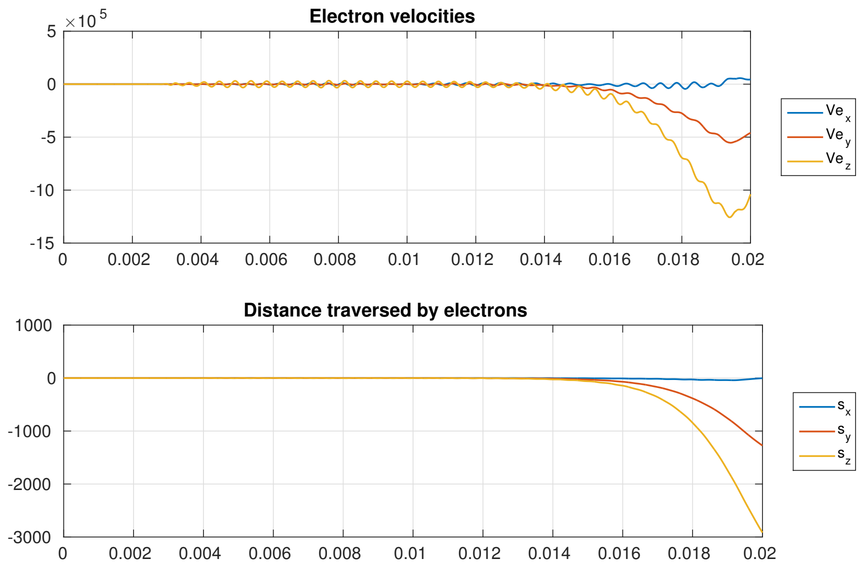

Figure A10: A plane wave source is located at $x = 0$ with a varying electric field E_z at $f = 2200$ Hz and an external magnetic field $B_{z0} = 40$ nT. The plasma frequency is $f_{\mathrm{pe}} = 1300$ Hz. Measured electron velocities inside the plasma region at $x = 780$ km with 120 macroparticles per cell.

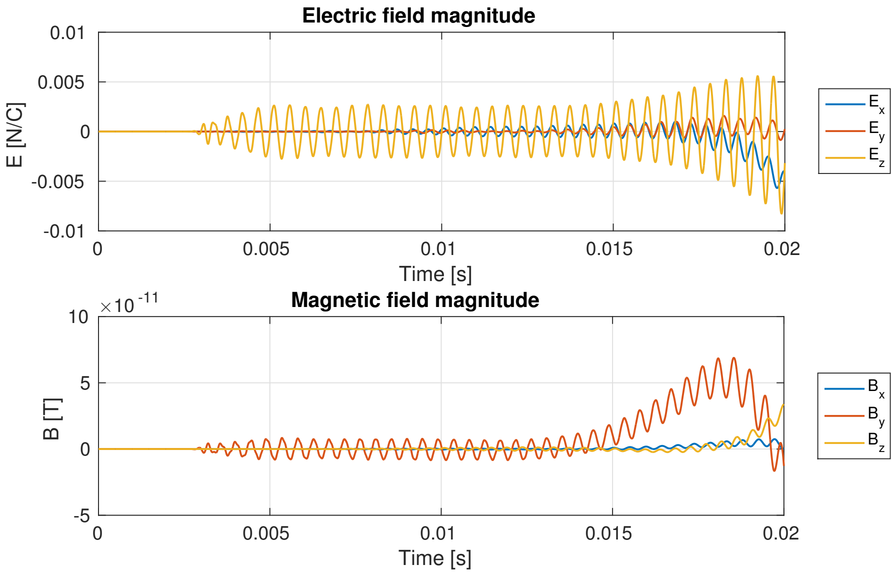

Figure A11: A plane wave source is located at $x = 0$ with a varying electric field E_z at $f = 2200$ Hz and an external magnetic field $B_{z0} = 40$ nT. The plasma frequency is $f_{\mathrm{pe}} = 1300$ Hz. Measured electric and magnetic field values inside the plasma region at $x = 780$ km with 200 macroparticles per cell.

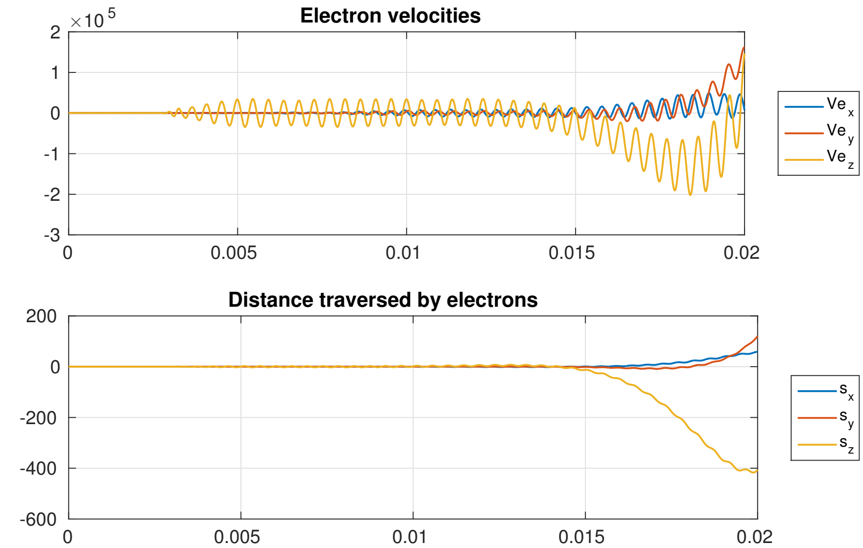

Figure A12: A plane wave source is located at $x = 0$ with a varying electric field E_z at $f = 2200$ Hz and an external magnetic field $B_{z0} = 40$ nT. The plasma frequency is $f_{\mathrm{pe}} = 1300$ Hz. Measured electron velocities inside the plasma region at $x = 780$ km with 200 macroparticles per cell.